QUADRUPOLE CENTRAL TRANSITION NMR SPECTROSCOPY OF

QUADRUPOLAR NUCLEI IN SOLUTION

By

JIAHUI SHEN

A thesis submitted to the Department of Chemistry

in conformity with the requirements for

the degree of Master of Science

Queen's University

Kingston, Ontario, Canada

September, 2016

Abstract

This thesis reports on ^{17}O (I = 5/2) and ^{59}Co (I = 7/2) quadrupole central transition (QCT) NMR studies of three classes of biologically important molecules: glucose, nicotinamide and Vitamin B_{12} derivatives. Extensive QCT NMR experiments were performed over a wide range of molecular motion by changing solvent viscosity and temperature. ^{17}O-labels were introduced at the 5- and 6-positions respectively: D-[5-^{17}O]-glucose and D-[6-^{17}O]-glucose following the literature method. QCT NMR greatly increased the molecular size limit obtained by ordinary solution NMR. It requires much lower temperatures to get the optimal spectral resolution, which are preferable for biological molecules. In addition, quadrupolar product parameter (P_Q) and shielding anisotropy product parameter (P_{SA}) were obtained for hydroxide group and amide group for the first time. For conventional NMR studies of quadrupolar nuclei, only P_Q is accessible while QCT NMR obtained both P_Q and P_{SA} simultaneously. Our experiments also suggest the resolution of QCT NMR can be even better than that obtained by conventional NMR. We observed for the first time that the second-order quadrupolar interaction becomes a dominant relaxation mechanism under ultraslow motion. All these observations suggest that QCT NMR can become a standard technique for studying quadrupolar nuclei in solution.

Acknowledgements

I would like to sincerely thank my supervisor, Dr. Gang Wu, for his generous help and patience during my study. This thesis would not be possible without his numerous assistance. I also appreciate the generous help from Dr. Xianqi Kong and Dr. Yin Gao in the lab. I hope to thank Dr. Francoise Sauriol, for her kind help in doing practical NMR experiments. I'm also very grateful to other lab mates in Dr. Wu's lab that make my master study experience unforgettable, I also appreciate the help from the undergraduate volunteer, Binyang Lin, for her assistance in glucose synthesis.

I would also like to express my gratitude to my friends in Suning Wang and Guojun Liu's Labs, i.e., Xiang Wang, Dengtao Yang, Kang Yuan and Heng Hu, Zijie Wang, Kaka Zhang, Shuaishuai Huang for their selfless help all through my studies as a master student. I would also like to thank Andrew Fraser from Mactarney's lab for his kind help in the lab.

Finally, I would like to thank my parents for their continuous support throughout my university years.

Table of Contents

List of Figures

List of Tables

List of Symbols and Abbreviations

Symbols

Å	angstrom
B_o	external magnetic field
C	boundary condition parameter
^oC	celsius
C_Q	quadrupole coupling constant
δ_{iso}	isotropic chemical shift
E	transition energy
f	shape factor
H	spin Hamiltonian
h	Planck's constant
I	nuclear spin number
k_B	Boltzmann constant
K	kelvin
m	magnetic quantum number
P_Q	quadrupole product parameter
P_{SA}	shielding anisotropy product parameter
r	molecular radius
$R_2{}^Q$	transverse relaxation rate
τ_c	correlation time
τ_o	rotational reorientation time at zero viscosity
T_1	spin-lattice relaxation time
T	temperature
μ	magnetic moment
$\Delta\nu_{1/2}$	line width
ν	NMR frequency
V_h	hydrodynamic volume
η_Q	asymmetry parameter
η	solvent viscosity
ω_0	Larmor angular frequency
ω_Q	nuclear quadrupole coupling constant, $\omega_Q = 2\pi C_Q$

Abbreviations

CT	central transition
CP	Cross-polarization
Ω	dynamic frequency shifts
DEAD	Diethyl azodicarboxylate
EFG	electric field gradient
kHz	kilohertz
MHz	megahertz
MAS	Magic angle spinning
NMR	Nuclear Magnetic Resonance
NAD	Nicotinamide Adenosine Dinucleotide
NADP	Nicotinamide adenine dinucleotide phosphate

ppm	parts per million
QCT	quadrupole central transition
QC	quadrupole coupling
Q	quadrupole interaction
Q2	second-order quadrupole interaction
SED	Stokes-Einstein-Debye
ST	satellite transition
SA	shielding anisotropy
T	tesla
VT	Variable temperature
χ_{ii}	three principal components of the quadrupolar coupling tensor

Chapter 1   Introduction

1.1   NMR Theory

Nuclear Magnetic Resonance (NMR) is a physical phenomenon that occurs when nuclei in an applied magnetic field absorb or emit certain amount of energy. The specific energy depends on the strength of the applied magnetic field and the magnetic properties of the target nuclei. Nowadays chemists use NMR spectroscopy as an analytical tool to study the physical and chemical properties of molecules based on the positions, intensities and fine structures of resonance peaks.

1.1.1   Nuclear Spin, Energy Levels and Transition Energy

For each nucleus, there is always an intrinsic value I associated that describes the spin of the nucleus. If the number of neutrons and the number of protons within the nucleus are both even, then the spins of individual protons and neutrons are paired against each other and thus no overall spin of the nucleus will appear. If the total number of neutrons and protons within the nucleus is odd, the nucleus has a half-integer spin I (i.e., 1/2, 3/2, 5/2). If the number of neutrons and the number of protons are both odd, then the nucleus has an integer spin I (i.e., 1, 2, 3). Quantum mechanics demonstrates that a nucleus of spin I will have $2I + 1$ possible spin states. When no external magnetic field is present, these spin states are degenerate. If a magnetic field is applied, the ground state will split into different energy levels proportional to the strength of the magnetic field. This is known as the Zeeman effect. Each energy level is associated with a magnetic quantum number, m $(m = I, I\text{-}1, ..., \text{-}I)$. Hence a nucleus with $I = 1/2$ will have two spin states, $m = \text{-}1/2$ and $+1/2$, when placed in a magnetic field, as shown in Fig. 1. The populations of the nuclei at different energy levels are determined by the Boltzmann distribution. At thermal equilibrium, there are more

nuclei at the lower energy level, and they can be excited to the higher energy level provided certain amount of energy is absorbed.
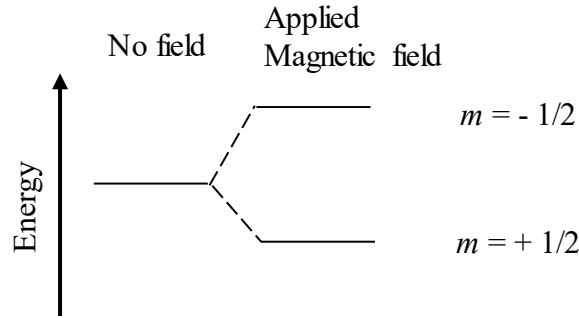
Figure 1. Zeeman Energy levels for a nucleus with spin number 1/2.

Since the nucleus has a positive charge and is spinning, it will generate a small magnetic field. The nucleus therefore possesses a magnetic moment, μ, which is proportional to its spin, I.

$$\mu = \frac{\gamma I h}{2\pi} \tag{1}$$

The constant γ is called the gyromagnetic ratio and is a fundamental nuclear constant which has a different value for every nucleus, and h is Planck's constant. The energy of a particular energy level is given by:

$$E = -\frac{\gamma h}{2\pi} m B_o \tag{2}$$

where B_o is the strength of the magnetic field at the nucleus. The energy difference between levels (i.e., the transition energy) with $\Delta m = \pm 1$ is

$$\Delta E = \frac{\gamma h B}{2\pi} \tag{3}$$

Hence when ΔE is absorbed by the nucleus, it will be excited to the higher energy level and then the NMR signal can be detected.

As shown in Fig. 2 (a), when a nucleus of spin 1/2 is at its lowest energy level, the nucleus will spin about its axis. When a magnetic field is applied, the axis of rotation will precess around the magnetic field. This frequency of precession is termed as the Larmor frequency, which is identical to the transition frequency.
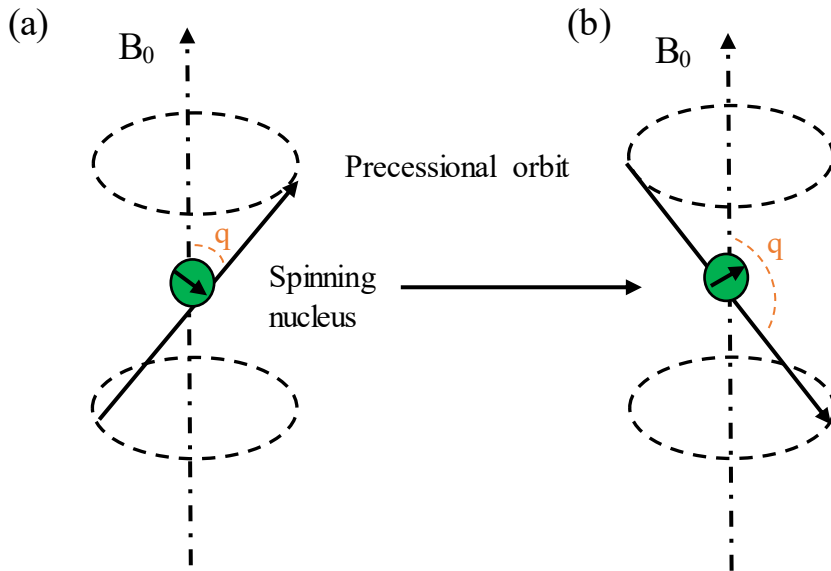
Figure 2. Larmor precession of the spin-1/2 nucleus around the magnetic field (a) before transition (b) after transition.

The potential energy of the precessing nucleus is given by:

$$E = -mB\cos q \tag{4}$$

where q is the angle between the direction of the applied field and the axis of nuclear rotation. If energy is absorbed by the nucleus, then the angle of precession, q, will change. As is shown in Fig. 2 (b), for a nucleus of spin 1/2, absorption of radiation "flips" the magnetic moment so that it opposes the applied field (the higher energy state). After this, without further energy input, gradually relaxation processes will occur which return the nuclei to the lower energy state.

1.1.2 Spin-lattice Relaxation and Spin-spin Relaxation

Spin-lattice relaxation is the mechanism by which the component of the magnetization vector along the direction of the static magnetic field reaches thermodynamic equilibrium with its surroundings (the "lattice"). It is characterized by the spin–lattice relaxation time, a time constant known as T_1. The vibrational and rotational motion of molecules in a sample will create a complex magnetic field. Since the sample environment around the nuclei has many different motions as well, when some of these components are equal in frequency and phase to the Larmor frequency of the nuclei of interest, they will then interact with nuclei in the higher energy state, and cause them to lose energy. The spin lattice relaxation time, T_1, is dependent on the gyromagnetic ratio of the nucleus and molecular motion.

Spin-spin (transverse) relaxation is a process where the transverse component of the magnetization vector exponentially decays towards its equilibrium value. It describes the interaction between neighbouring nuclei with identical precessional frequencies but different magnetic quantum states. A nucleus in the lower energy level will be excited, while the excited nucleus relaxes to the lower energy state. There is no net change in the populations of the energy states in this process, but the average lifetime of a nucleus in the excited state will decrease. It is characterized by the spin–spin relaxation time, known as T_2. This parameter is often related to the line width ($\Delta\nu_{1/2}$) of the NMR signal, which has a Lorentzian line shape in the following fashion:

$$\Delta\nu_{1/2} = \frac{1}{\pi T_2} \tag{5}$$

1.1.3 NMR Interactions

1.1.3.1 The Zeeman Interaction

The Zeeman interaction is the most fundamental interaction among all the NMR interactions. It is the interaction between the nuclear magnetic moment and the applied magnetic field. There are also several magnetic and electronic interactions coupling with the nucleus, with which structural and dynamic information may be obtained. However, since the Zeeman interaction is the largest, followed by the quadrupolar interaction, and then followed by chemical shift and the dipolar coupling, the other interactions can usually be viewed as perturbations to the Zeeman interaction. Hence the full NMR Hamiltonian can be written as

$$H = H_Z + H_Q + H_{CS} + H_{DD} + H_J \tag{6}$$

where H_Z is the Zeeman interaction, H_Q is the quadrupolar coupling, H_{CS} is the chemical shift coupling, H_{DD} is the dipolar coupling and H_J is the J coupling. The relative magnitude of these interactions is given in Table 1.

Table 1. Typical magnitude of different NMR interactions.

Interaction	Magnitude
Zeeman	100-1000 MHz
Quadrupolar	1-10 MHz
Chemical Shift	20 kHz
Dipolar interaction	50 kHz
J-coupling	1-100 Hz

1.1.3.2 Chemical Shift

Chemical shift is the resonant frequency of a nucleus relative to a standard in a magnetic field, which appears because the magnetic field the nucleus feels is usually not equal to the applied magnetic field, as electrons around the nucleus will shield or deshield it from the applied field. For

example, in Fig. 3, since the electron around the nucleus will create a magnetic field that opposes to the applied magnetic field (i.e. shielding effect), the effective magnetic field applied to the nucleus is smaller than the external magnetic field. Nowadays, chemical shift (δ) is defined in the following way:

$$\delta = \frac{\nu_{sample} - \nu_{ref}}{\nu_{ref}} \tag{7}$$

where ν_{sample} is the absolute resonance frequency of the sample and ν_{ref} is the absolute resonance frequency of a standard reference compound. For example, in ^1H NMR, the reference is usually tetramethylsilane, $Si(CH_3)_4$.
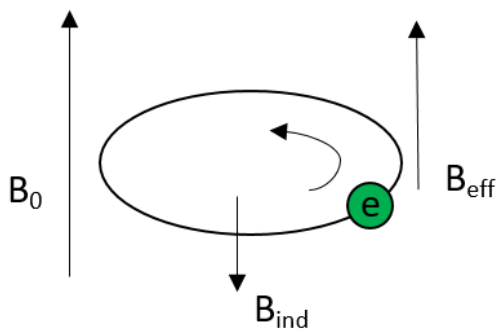
Figure 3. Shielding of the electron in the applied magnetic field.

A number of factors can cause chemical shifts, such as electron density, electronegativity of neighboring groups and anisotropic induced magnetic field effects. By studying chemical shifts, lots of information such as bond lengths and angles, bond types and coordination environments can be obtained.

1.1.3.3 *J*-Coupling

J-coupling is also known as scalar coupling or spin-spin coupling. It is an indirect interaction between two nuclear spins. It contains information about detailed structures of

molecule, such as bond distance and angles, or the connectivity of molecules. Since each nucleus can be viewed as a small magnet, the orientation of that magnet has an effect on the local magnetic field experienced by other nuclei. Therefore, different connecting environments yield different spin-spin coupling constants. The *J*-coupling is mediated through bonds, usually within 3 chemical bonds.

1.1.3.4 Dipolar Coupling

Dipolar coupling is a through-space coupling of two NMR active nuclei, which is the magnetic effect on nucleus *I* due to the magnetic field generated by nucleus *S*, as shown in Fig. 4. The dipolar coupling of spins is either between two of the same nuclei (homo-nuclear dipolar coupling) or between two different nuclei (heteronuclear dipole coupling). The size of dipolar coupling is mostly affected by the distance between the nuclei. The dipolar coupling constant is known as

$$R = \frac{\mu_0 h}{4\pi} \frac{\gamma_I \gamma_S}{r^3} \tag{8}$$

where μ_0 is the vacuum permeability, h is the Planck's constant, r is the distance between nuclei I and S, and γ_I and γ_S are the gyromagnetic ratio of I and S respectively.
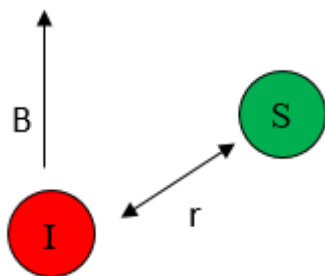
Figure 4. Dipolar coupling between two spatially close nuclei.

1.1.3.5 Quadrupolar Coupling

Apart from the magnetic dipole moment, an electric quadrupole moment also needs to be considered for NMR active nuclei that have spin number I > 1/2. It is the interaction between the quadrupolar moment and the electric field gradients (EFG) generated by their surroundings. As shown in Fig. 5, if a nucleus is spin-1/2, the positive charge is spherically distributed in the nucleus and consequently vanishing quadrupolar moment. However, when I > 1/2, the positive charge distribution in the nucleus is no longer spherical and is orientational sensitive. Hence the EFG will interact with the nuclei and create a torque on the nucleus and thus quadrupolar coupling occurs.
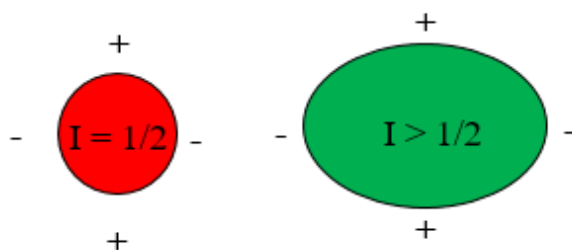
Figure 5. Nuclear charge distribution for a spin 1/2 nucleus (red circle) and a quadrupolar nucleus (green oval).

For example, ^{14}N is a $I = 1$ nucleus and thus is quadrupolar. Therefore, the charge distribution around the nucleus is not symmetrical and the quadrupolar interaction significantly broadens the linewidth of the signal. The more asymmetric the environment is, the more broad the signal will be. Fig. 6 shows the effect of asymmetry on the ^{14}N NMR spectra. The symmetric NH_4^+ and the Me_4N^+ gives the sharpest signal while other ammonium ions give broad and unresolved signals.[1]

The quadrupolar interaction is the largest interaction in NMR apart from the Zeeman interaction and they sometimes even can become comparable in size. Due to this reason, the quadrupolar interaction cannot be treated with just the first order like most of the other interactions. Sometimes both first and second order quadrupolar interactions need to be considered.[2]

^1J (^{1}H, ^{14}N)
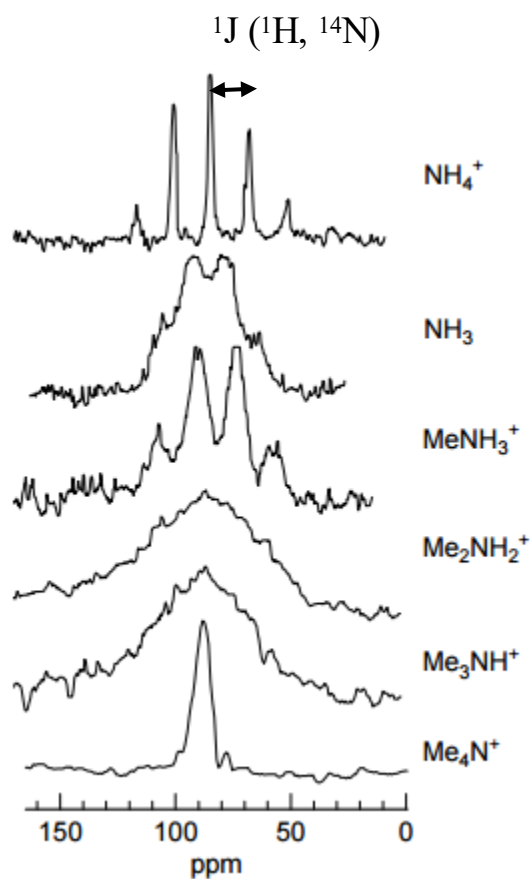
Figure 6. ^{14}N NMR spectra of a series of ammonia samples in solution. The figure was reproduced from Ogg and Ray.[1]

1.2   Spin-1/2 NMR

Spin-1/2 nuclei such as (^{13}C and ^{1}H) are widely used for structure determination as they usually give sharp lines and easily observed *J*-coupling. In the liquid state, the dipolar and anisotropic contribution to the chemical shift are averaged to zero due to the molecular reorientation occurring in liquids, resulting in the characteristically narrow isotropic peaks. Some spin-1/2 nuclei have high natural abundance. For example, ^{1}H, ^{19}F, and ^{31}P all have a 100% abundance.

1.3   Quadrupole NMR

Quadrupolar nuclei (I > ½) such as ^{14}N (I = 1), ^{23}Na (I = 3/2), ^{17}O (I = 5/2) and ^{59}Co (I = 7/2), although forming the majority of the NMR active nuclei, are far less commonly used in NMR studies. The primary difficulty with quadrupole NMR is that the spin-spin relaxation time can be very short, resulting in broad lines. Since T_2 is determined by two factors: (a) the electric quadrupole moment (Q), (b) the presence of electric field gradients (EFG) at the nucleus. To improve the spectral resolution, one may firstly focus on quadrupolar nuclei with small electric quadrupole moments (Q) far less than l. Usually the NMR signals are relatively sharp for ^2H (Q = + 0.003), ^6Li (Q = - 0.0008), ^{11}B (Q = + 0.04). Secondly, in order to minimize the EFG coupling, molecules with high symmetry (tetrahedral and octahedral) in which the target quadrupolar nucleus is at the center of symmetry are used and thus can give sharp lines and J-multiplets as discussed earlier; Fig. 6. In solution-state NMR, one common approach for improving the resolution of quadrupolar nuclei is to collect spectra at elevated temperatures where molecular reorientational correlation times are much shorter, and thus the quadrupolar broadening is reduced. Unfortunately, the temperature needed to reach this motional narrowing regime is often impractically high for many samples.

1.3.1   Solid-State NMR

In practice, large molecules such as proteins and nanoparticles usually have low solubility in common NMR solvents and thus conventional solution-state NMR is not applicable. In that case, solid-state NMR becomes a necessary method to obtain molecular dynamic information. Solid-state NMR is a quite different technique from solution-state NMR. As molecules in the solid state are rigid, anisotropic spin interactions cannot be averaged out as the case in liquid solutions.

This results in extensively broadened NMR signals to over 1 MHz wide, even larger than the bandwidth of most NMR spectrometers. For example, Fig. 7 shows the solution-state and solid-state ^{13}C NMR of glycine.[3] All the anisotropic interactions are averaged out in aqueous solutions, giving sharp well-resolved signals. In solid-state NMR, however, the same compound gives much broader signal (~200 ppm), which is due to the dipolar couplings and the chemical-shift anisotropy. Several technologies such as Cross Polarization (CP), Magic Angle Spinning (MAS) and Multidimensional NMR and Multipulse Decoupling have been applied to improve the resolution of solid-state NMR.[4] Solid-state NMR was also applied to quadrupolar nuclei such as ^{17}O, ^{67}Zn, ^{59}Co, ^{23}Na, and ^{39}K in biological systems due to these technology improvements.[5]
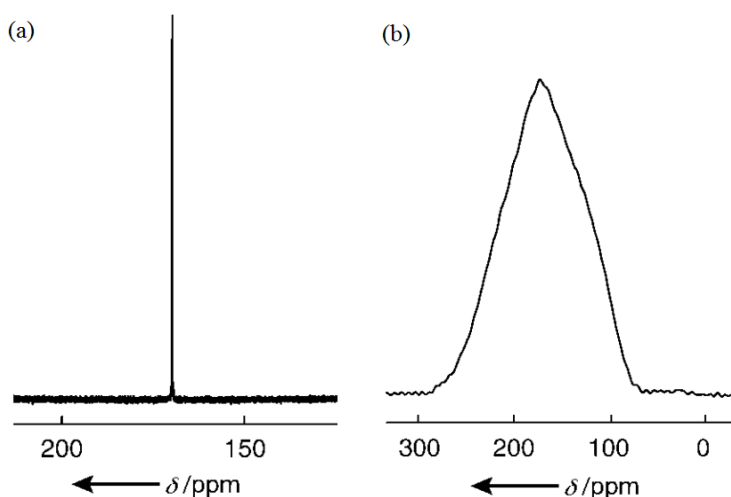
Figure 7. (a) Liquid-state ^{13}C NMR spectrum (75 MHz) of 10 mM 1-^{13}C labeled (10%) glycine in H$_2$O. (b) Solid-state ^{13}C NMR spectrum (125 MHz) of 1-^{13}C labeled (10%) glycine powder (90 mg). The figure was reproduced from Laws *et al.*[3]

1.3.2 Quadrupole Central Transition (QCT) NMR

Due to those constraints of solid-state NMR, although it can yield a lot of useful information, conducting quadrupolar NMR experiments in aqueous solution is still highly desirable, as it would enable scientists to directly study the interactions between macromolecules

11

in biological systems under physiologically relevant conditions for those biologically important quadrupolar nuclei, such as ^{17}O and ^{59}Co. Well established theories dating back several decades ago state that transverse relaxation process of a half-integer spin exhibits multi-exponential relaxation characteristics[6,7] and only the central transition (CT) signal can be detected under the slow motion condition ($\omega_0\tau_c \gg 1$, where ω_0 is the angular Larmor frequency of the nucleus under detection and τ_c is the molecular rotational correlation time) as it can have relatively long transverse relaxation times under that condition. This NMR method that particularly focuses on detection of the CT signals, was termed quadrupole central transition (QCT) spectroscopy in the literature.[8]

Oldfield *et al.*[9] first reported ^{17}O NMR spectra for $C^{17}O$ NMR signals for $C^{17}O$ ligands bound to proteins (peroxidases, myoglobins, and hemoglobins) in aqueous solution. However, since the nuclear quadrupole coupling constant (C_Q) for $C^{17}O$ is extremely small ($C_Q < 1$ MHz), it was still not clear whether the multi-exponential relaxation properties of ^{17}O can be generalized as a standard method for studying other oxygen-containing functional groups that usually have much larger C_Q values (ca. $C_Q = 6\text{-}20$ MHz). Vogel *et al.* also applied this method to detect metal ions such as ^{51}V (spin-7/2), ^{27}Al (spin-5/2), ^{45}Sc (spin-7/2), $^{69,71}Ga$ (spin-3/2) bound to large proteins,[10-14] and obtained quadrupole coupling constant (C_Q) and rotation correlation time (τ_c) in these systems. However, although this relaxation behavior of the quadrupolar nuclei has been known for decades, its importance in NMR studies was not widely valued. There had been no follow-up QCT NMR studies for biological macromolecules in aqueous solutions for more than 20 years. Recently, Zhu and Wu[15,16] increased the size limit of molecular systems previously attainable by solution ^{17}O NMR by 1000 fold using QCT method. They showed that ^{17}O QCT NMR spectroscopy is applicable even when the quadrupolar coupling constant of the molecule is in the 5-10 MHz range

typical of many organic compounds. Shielding anisotropy parameters were also obtained, indicating that QCT NMR spectroscopy can be a standard technique to obtain high-resolution ^{17}O NMR spectra for large biological micromoles in aqueous solution. Following them, there has been a renewed interest in NMR studies of half-integer quadrupolar nuclei such as ^{17}O in liquids under slow motion conditions. Mueller *et al.[17]* showed that solution-state ^{17}O QCT NMR spectroscopy can be used to characterize enzymatic intermediates with active catalysis, catching kinetically competent intermediates in the act of chemical transformation, which showed the great potential for ^{17}O QCT NMR as a probe to characterize bio-molecular systems. Zhu *et al.*[18] also provided the direct experimental NMR relaxation data over a wide range of motion. They showed that the quadrupole transverse relaxation increases with the rotational correlation time (τ_c) of the molecules in liquids (i. e., the tumbling motion of molecules) until it reaches a maximum at $\tau_c \approx 1/\omega_0$. As the molecular motion is further slowed down, only the central transition is observed and its transverse relaxation rate decreases drastically as τ_c increases. This is generally true when $\omega_0\tau_c \approx (\omega_0/\omega_Q)^2$, where ω_Q is the nuclear quadrupole coupling constant in angular frequency unit (i.e., $\omega_Q = 2\pi C_Q$). However, previous workers[2,7,19] predicted that, when the molecular motion becomes ultraslow (e.g., $\omega_0\tau_c > (\omega_0/\omega_Q)^2$), the second-order quadrupole interaction experienced by the CT should become a dominant factor for the transverse relaxation rate and thus with the increase of τ_c, so does the quadrupole transverse relaxation rate. Lately, Wu[20] proposed an approximate analytical expression that can be used to analyze nuclear quadrupole transverse relaxation data of any half-integer spin in liquids over the entire motional range including the ultraslow motion range. The proposed equation yields results that are in excellent agreement with the exact numerical calculation, making the choosing of most optimal condition for getting best resolution more practical.

1.3.3 Molecular Rotational Dynamics in Solution

In QCT NMR studies, it is often necessary to know the molecular rotational correlation time τ_c. This parameter is used to describe the rotational dynamics of molecules in solution. The Stokes-Einstein-Debye (SED) equation can be usually used as the simplest model for medium sized molecules (of a few hundred Å^3 volumes):

$$\tau_c = \frac{V_h \eta}{k_B T} \tag{9}$$

where V_h is the hydrodynamic volume of the molecule under study, η is the solvent viscosity, k_B is the Boltzmann constant, and T is the absolute temperature of the sample.

In some cases, a modified SED equation is used to describe the rotational dynamics for any general molecule[21]

$$\tau_c = \frac{V_h fC\eta}{k_B T} \tag{10}$$

where f is referred to as a shape factor and is well specified, C is the boundary condition parameter dependent strongly on solute and solvent molecules. For solute molecules that are significantly larger than the solvent molecules, it is considered that the target solute lies in the stick limit, which means the first solvent shell coherently rotates with the probe molecule.[21] In this case, there is a strong coupling between solvent and solute along the surface tangent and C is considered to be equal to 1. Hence eq. (10) can be reduced to eq. (9) under this condition. For solute molecules whose size is comparable to or less than that of solvent molecules, it is considered that the rotation is in the slip limit mode, which means the solute molecules only rotate on their own in the cavity of solvent molecules. Solvent is assumed not to rotate with the probe molecules, hence the resistance to the motion arises from the displacement of the solvent molecule as the non-spherical molecules rotates. Usually, C is considerably smaller than 1 in this condition.[21]

1.4   Objectives of the Thesis

In this thesis, we carried out extensive experimental QCT NMR studies for two biologically important quadrupolar nuclei ^{17}O and ^{59}Co. Whenever possible, molecules of interest are studied over the entire motional range to better understand the spectral characteristics of QCT NMR signals. From these QCT NMR studies, NMR parameters such as isotropic chemical shifts (δ_{iso}), quadrupole product parameter (P_Q) and shielding anisotropy product parameter (P_{SA}) will be conveniently determined.

Chapter 2   QCT Theory

2.1   Quadrupole Relaxation Processes

The Redfield's relaxation theory[6] suggests that the transverse relaxation process of a half-integer quadrupole nucleus is multi-exponential, and thus the resultant NMR spectrum consists of $(I + 1/2)$ components arising from one central-transition (CT, $m = +1/2 \leftrightarrow -1/2$) and $(I - 1/2)$ pairs of satellite transitions (STs, e.g., $m = \pm 3/2 \leftrightarrow \pm 1/2, \pm 5/2 \leftrightarrow \pm 3/2$, etc.). For example, for a nuclear spin system containing spin-5/2 nuclei, such as ^{17}O, the nuclear Zeeman energy levels are shown in Fig. 8, which contains one CT and two pairs of STs.

m

-5/2	
	ST$_2$
-3/2	
	ST$_1$
-1/2	
	CT
1/2	
	ST$_1$
3/2	
	ST$_2$
5/2	
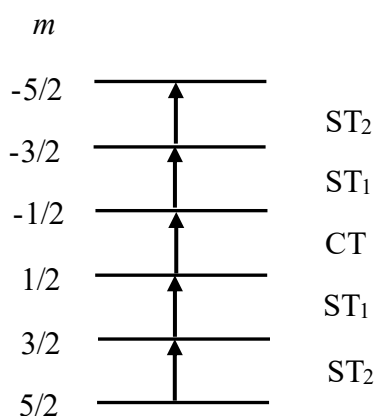
Figure 8. Zeeman energy levels and state labels for $I = 5/2$ nuclei. CT = central transition, ST$_1$ = first satellite transition, and ST$_2$ = second satellite transition.

It is also known that among these $I + 1/2$ exponential components, the CT can have relatively long transverse relaxation time in the slow motion limit. For example, for a spin-5/2 nucleus, only the central transition relaxation is of reasonable range to be detected while both the first and second satellite transitions relaxation rate are too large to detect. Hence, by detecting CT signals under the slow motion limit, relatively narrow lines can be obtained in NMR spectra of

half-integer quadrupolar nuclei in solution. As discussed in the previous chapter, to date only a few QCT NMR studies have been reported in the literature. In NMR experiments of liquid samples where molecules undergo isotropic tumbling, the quadrupole interaction is often the predominant relaxation mechanism and is usually described by a second-rank tensor known as the quadrupole coupling (QC) tensor whose three principal components are defined as χ_{ji} ($ii = xx, yy$, and zz, and $|\chi_{zz}| > |\chi_{yy}| > |\chi_{xx}|$). In general, the two quantities that can be directly determined from NMR spectra are the nuclear quadrupole coupling constant (C_Q) and the asymmetry parameter (η_Q):

$$C_Q = \chi_{zz} \tag{11}$$

$$\eta_Q = \left(\frac{\chi_{xx} - \chi_{yy}}{\chi_{zz}}\right) \tag{12}$$

Since usually these two quantities are coupled together, especially in the quadrupole relaxation process, another parameter, P_Q, known as the quadrupole product parameter, is defined in the following way:

$$P_Q = C_Q\sqrt{1 + \frac{\eta_Q^2}{3}} \tag{13}$$

Under the fast motion condition (also known as the extreme narrowing condition), $\omega_0\tau_c \ll 1$, all ($I + 1/2$) components have the same transverse relaxation rate (R_2^Q), resulting in a singly Lorentzian signal with its line width given by:[22]

$$\Delta\nu_{1/2}^Q = \frac{R_2^Q}{\pi} = \frac{3\pi}{10}\frac{2I+3}{I^2(2I-1)}P_Q^2\tau_c \tag{14}$$

where P_Q is the quadrupole product parameter and τ_c is the molecular rotational correlation time.
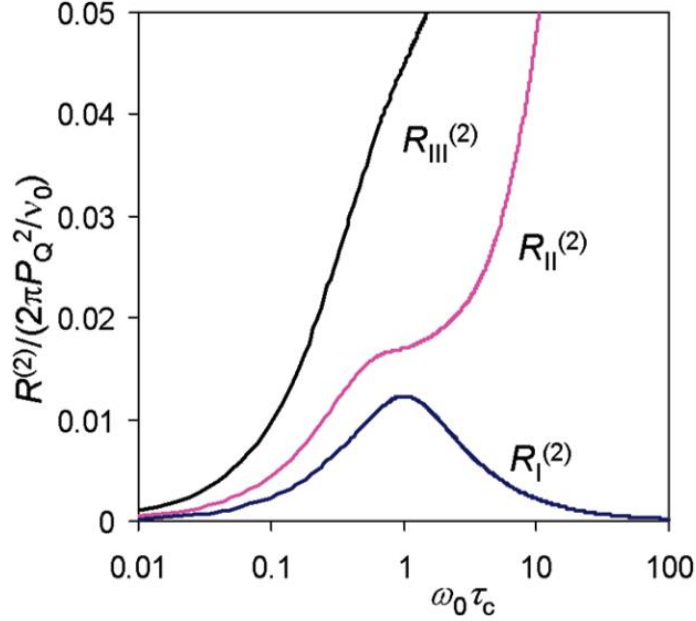
Figure 9. Theoretical results for transverse relaxation rate for spin-5/2 nuclei. The figure was reproduced from Zhu and Wu.[15] R_I, R_{II} and R_{III} are the relaxation rates of CT, ST$_1$ and ST$_2$ respectively.

When the molecular tumbling motion is in the intermediate regime where $\omega_0\tau_c \approx 1$, a multi-Lorentzian line shape begins to exhibit in the NMR signal of a half-integer quadrupolar. Under this range, exact analytical expressions for individual quadrupole relaxation rates exist only for $I = 3/2$.[23,24] For $I > 3/2$, one generally has to carry out numerical diagonalization of the Redfield relaxation matrix.[25] However, in practice, especially for high I spins, the STs are broadened so quickly in the slow motion range as τ_c increases that the observable NMR signal over a wide range of motion can always be reasonably modeled by a Lorentzian line shape. Recently, Wu[20] proposed an approximate analytical expression to describe the line width of the observable NMR signal due to the quadrupole transverse relaxation over the entire motional range including the ultraslow range:

$$\Delta\nu_{1/2}^Q = \frac{R_2^Q}{\pi} = \frac{3\pi}{20}\frac{2I+3}{I^2(2I-1)}P_Q{}^2[J(\omega_0) + J(2\beta\omega_0)] \tag{15}$$

18

where $J(\omega)$ is the normalized spectral density function defined as:

$$J(\omega) = \frac{\tau_c}{1 + \omega_0^2 \tau_c^2} \tag{16}$$

and

$$\beta = \sqrt{\frac{2}{I(I+1) - \frac{7}{4}}} \tag{17}$$

Thus β is equal to 1, $(2/7)^{1/2}$, $(2/14)^{1/2}$, and $(2/23)^{1/2}$ for $I = 3/2$, $5/2$, $7/2$ and $9/2$, respectively. It is apparent that eq. (15) is reduced to eq. (14) under the extreme narrowing condition. It should be noted that eq. (15) is valid within the limit of Redfield's relaxation theory. When the molecular motion becomes ultraslow so that1 $\omega_o\tau_c > (\omega_o/\omega_Q)^2$, it was predicted decades ago that the second-order quadrupole interaction should become a dominant factor for the transverse relaxation rate of the CT.[7,19,26] The analytical expression of the second-order quadrupole contribution to the line width was reported by following Werbelow[2] as:

$$\Delta_{1/2}^{Q2} = \frac{R_2^{Q2}}{\pi} = \frac{36\pi}{16 \times 16} \left[\frac{I(I+1) - 3/4}{I^2(2I-1)^2}\right]^2 \left[\frac{2086}{6125}\right] \left(\frac{P_Q^2}{\nu_0}\right)^2 J(0) \tag{18}$$

Eq. (18) suggests that the contribution of the second-order quadrupole interaction to the line width increases with τ_c under the ultraslow motion. Since it is inversely proportional to $(\nu_0)^2$, very high magnetic fields need to be applied to suppress this contribution.

Apart from the quadrupole relaxation process, it is well known that the shielding anisotropy (SA) also contributes to the line width and this SA contribution can be written as:[26]

$$\Delta_{1/2}^{SA} = \frac{R_2^{SA}}{\pi} = \frac{2\pi}{45} (P_{SA}\nu_0)^2 \big(8J(0) + 6J(\omega_0)\big) \tag{19}$$

where the shielding anisotropy product parameter (ppm, 10^{-6}), P_{SA}, is defined as

$$P_{SA} = \Delta\sigma \sqrt{1 + \frac{\eta_{SA}^2}{3}} \tag{20}$$

$\Delta\sigma$ and η_{SA} are related to the shielding tensor components (σ_{xx}, σ_{yy}, and σ_{zz} defined according

to $|\sigma_{zz} - \sigma_{iso}| \geq |\sigma_{xx} - \sigma_{iso}| \, |\sigma_{yy} - \sigma_{iso}|$) in the following way:

$$\Delta\sigma = \sigma_{zz} - \frac{\sigma_{xx} + \sigma_{yy}}{2} \tag{21}$$

$$\eta_{SA} = \frac{\sigma_{yy} - \sigma_{xx}}{\sigma_{zz} - \sigma_{iso}} \tag{22}$$

Since the contribution from SA to the NMR line width is proportional to $J(0) = \tau_c$, it may become important when the molecular motion slows down, especially at high magnetic fields.

Thus the total line width of the NMR signal for any half-integer spin in any motional regime of isotropic liquids can be written as:

$$\Delta\nu_{1/2}^{total} = \Delta\nu_{1/2}^{Q} + \Delta\nu_{1/2}^{Q2} + \Delta\nu_{1/2}^{SA} \tag{23}$$

The detailed equation is

$$\text{Linewidth} = \frac{3\pi}{20} \times \frac{2I+3}{I^2 \times (2I-1)} \times P_Q^{\ 2} \times \left(\frac{\tau_c}{1 + \omega_o^{\ 2}\tau_c^{\ 2}} + \frac{\tau_c}{1 + \frac{8}{I(I+1) - \frac{7}{4}}\omega_o^{\ 2}\tau_c^{\ 2}} \right) + \frac{36\pi}{16 \times 16} \times$$

$$\left(\frac{I(I+1) - 3/4}{I^2(2I-1)^2} \right)^2 \times \left(\frac{2086}{6125} \right) \times \left(\frac{P_Q^{\ 2}}{\nu_0} \right)^2 \times \tau_c + \frac{2\pi}{45} \times (P_{SA} \times \nu_o)^2 \times \tau_c \times \left(8 + \frac{6}{1 + \omega_o^{\ 2}\tau_c^{\ 2}} \right) \tag{24}$$

By fitting the experimental data using this field-dependent line shape, the extraction of quadrupole product parameter (P_Q) and shielding anisotropy product parameter (P_{SA}) become possible. For conventional NMR studies of quadrupolar nuclei, only P_Q is accessible. Of course, other relaxation mechanisms such as dipole-dipole and J-coupling interactions can be further added to eq. (23). But in practice, the Q, Q2 and SA contributions are the most important ones for half-integer quadrupolar nuclei.

Using typical ^{17}O NMR parameters, we illustrate in Fig. 10 how the three different contributions (Q, Q2 and SA) to the NMR line width vary as a function of $\omega_o\tau_c$. In Fig. 10, the range of $\omega_0\tau_c$ covers 7 orders of magnitude. In the extremely narrowing regime where $\omega_o\tau_c \ll 1$, the quadrupole interaction (Q) is dominating and causes the line width of the NMR signal to reach

a maximum at around $\omega_0\tau_c = 1$. In the slow motion regime where $\omega_0\tau_c > 1$, usually only the CT can be detected and its line width arising from the Q contribution decreases with the increase of $\omega_0\tau_c$. When the molecular motion becomes so slow that $\omega_0\tau_c$ is greater than $(\omega_o/\omega_Q)^2$, the second-order quadrupole interaction (Q2) contribution begins to become predominant and increases with τ_c. As seen from Fig. 10, the SA contribution, while displaying a similar dependence on τ_c in the slow motion regime, is much smaller than the Q2 contribution for the particular set of ^{17}O NMR parameters chosen. However, as reported previously,[9,18] for some oxygen-containing functional groups, the SA contribution to the line width can be considerably larger than the Q2 contribution in the ultraslow motion regime. This is also particularly true at very high magnetic fields because the SA factor increases with ν_0 whereas the Q2 interaction is inversely proportional to ν_0, the Larmor frequency of the nucleus under detection.
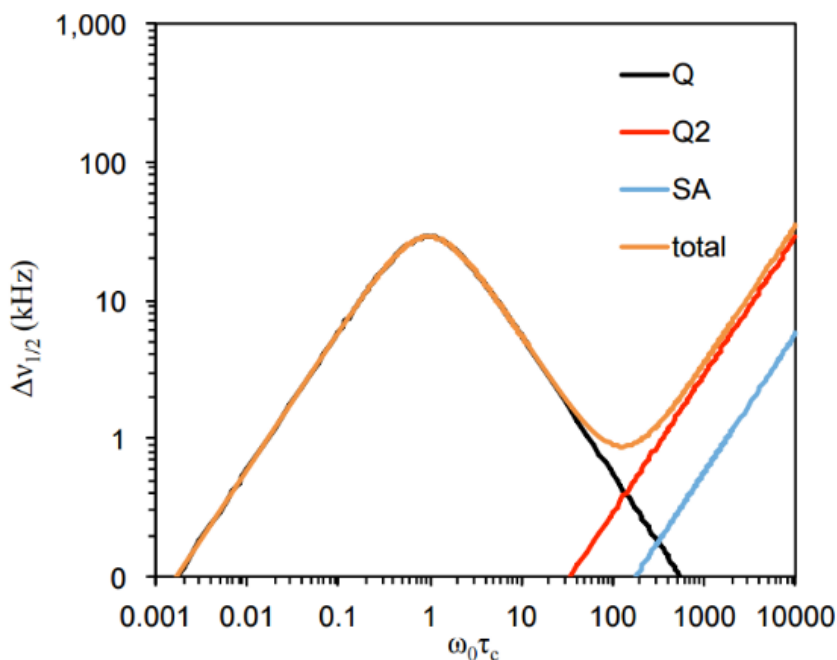
Figure 10. Illustration of contributions from the quadrupole (Q), second-order quadrupole (Q2) and shielding anisotropy (SA) interactions to the line width as a function of $\omega_0\tau_c$. The following ^{17}O NMR parameters were used in the calculations: $I = 5/2$, $P_Q = 10$ MHz, $\nu_0 = 81$ MHz, and $P_{SA} = 200$ ppm.

2.2   Dynamic Frequency Shifts

One of the noticeable features of QCT NMR is that the peak position of the central transition is perturbed from the true chemical shift by a 2nd order magnetic-field dependent frequency shift. For $I = 5/2$, the analytical expressions for dynamic (angular) frequency shifts have been given previously by Werbelow:[27]

$$\Omega_I = \frac{3\pi^2}{1000} P_Q^2(-16Q_1 + 16Q_2) \tag{25}$$

$$\Omega_{II} = \frac{3\pi^2}{1000} P_Q^2(-4Q_1 + 10Q_2) \tag{26}$$

$$\Omega_{III} = \frac{3\pi^2}{1000} P_Q^2(32Q_1 - 8Q_2) \tag{27}$$

where Ω_I, Ω_{II}, and Ω_{III} are the dynamic frequency shifts for CT, ST_1, ST_2, respectively. Q_n ($n = 1$, 2) is the imaginary part of the normalized spectral density function and is related to the real part of the function, J_n ($n = 0, 1, 2$), in the following way:

$$Q_n = n\omega_o\tau_c J_n \tag{28}$$

$$J_n = \frac{\tau_c}{1+(n\omega_o\tau_c)^2} \tag{29}$$

It is often more common to define the dynamic frequency in parts per million to be consistent with the chemical shift scale:

$$\Delta\delta_d = \frac{\Omega}{2\pi\nu_0} \times 10^6 \tag{30}$$

where ν_0 is the Larmor frequency of the nucleus under detection, $\nu_0 = \omega_0/2\pi$. For QCT NMR spectroscopy, only the central transition is observed and thus the dynamic frequency shift (ppm) is then given by

$$\Delta\delta_d = \delta_{obsd} - \delta_{iso} = \frac{\Omega_I}{2\pi\nu_0} \times 10^6 \approx (-6 \times 10^3)(\frac{P_Q}{\nu_o})^2 \tag{31}$$

where δ_{obsd} is the observed QCT signal position (ppm), and δ_{iso} is the isotropic chemical shift (ppm).
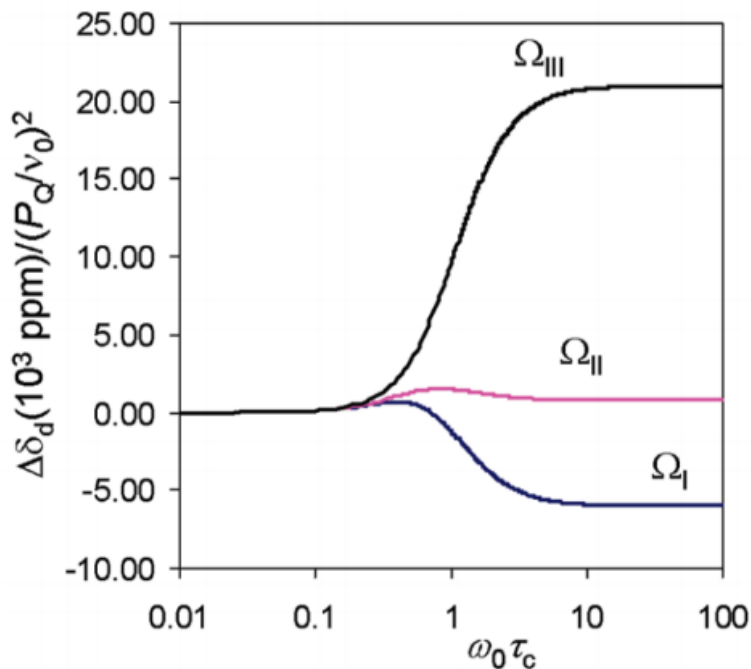
Figure 11. Theoretical results for dynamic frequency shifts for spin-5/2 nuclei. The figure was reproduced from Zhu and Wu.[15]

Fig. 11 shows the theoretical results for dynamic frequency shifts for spin-5/2 nuclei. $\Delta\delta_d$ for the CT (Ω_I) is nearly always negative whereas $\Delta\delta_d$ for the ST_1 (Ω_{II}) is essentially negligible. Although $\Delta\delta_d$ for the ST_2 (Ω_{III}) is much larger than those for the other two components, it can never be observed in practice either because of its negligible amplitude or because of its excessive line width, as is demonstrated in Zhu and Wu.[15] Therefore, it can be easily inferred that the observed QCT signal always appears at a lower frequency position from the true isotropic chemical shift position. Eq. (31) indicates that the quadrupole product parameter P_Q and the isotropic chemical shift δ_{iso} can be obtained by doing measurements at multiple magnetic fields.

2.3 Spectral Intensity and Nutation Behavior of QCT Signals

It is also known that the effective 90° pulse width for the CT signal is $I + 1/2$ times shorter than that of a conventional 90° pulse, and the relative spectral intensity of the CT signal is given by the following equation:[15]

$$\frac{I_{CT}}{I_{conventional}} = \frac{3}{4I(I+1)} \tag{32}$$

Hence for spin-5/2 nuclei such as ^{17}O, eq. (32) suggests that the maximum CT signal generated by a single RF pulse is only $3/35 \approx 8.6\%$ of the total signal intensity under the selective excitation condition, and for spin-7/2 nuclei such as ^{59}Co, it would be $1/21 \approx 4.8\%$.

2.4 Optimal Resolution in QCT Spectra

To further examine the line width of the observable NMR signal due to the quadrupole transverse relaxation, we use ^{17}O (I = 5/2) as an example. Fig. 12 shows the contour of line width in the ν_0-τ_c space for several typical combinations of P_Q and P_{SA}: (a) $P_Q = 2$ MHz and $P_{SA} = 1000$ ppm, typical of metal-oxo groups;[28] (b) $P_Q = 8$ MHz and $P_{SA} = 500$ ppm, typical of amide and peptides;[29,30] (c) $P_Q = 13$ MHz and $P_{SA} = 200$ ppm, typical of -OH groups;[31-33] (d) $P_Q = 16$ MHz and $P_{SA} = 3000$ ppm, typical of nitroso functional groups.[32] For all the plots in Fig. 12, there is always a ridge along the line of $\omega_0\tau_c = 1$. On the left-hand side of this ridge ($\omega_0\tau_c < 1$), the molecular tumbling motion is in the fast regime, and particular values of P_Q and P_{SA} would yield distinct line width. However, in the slow motion regime, the line width landscape always exhibits a valley in the region between $\omega_0\tau_c \approx 10$ and $\omega_0\tau_c \approx 100$. These findings suggest those valley areas would be the optimal regions to perform QCT NMR in practice.
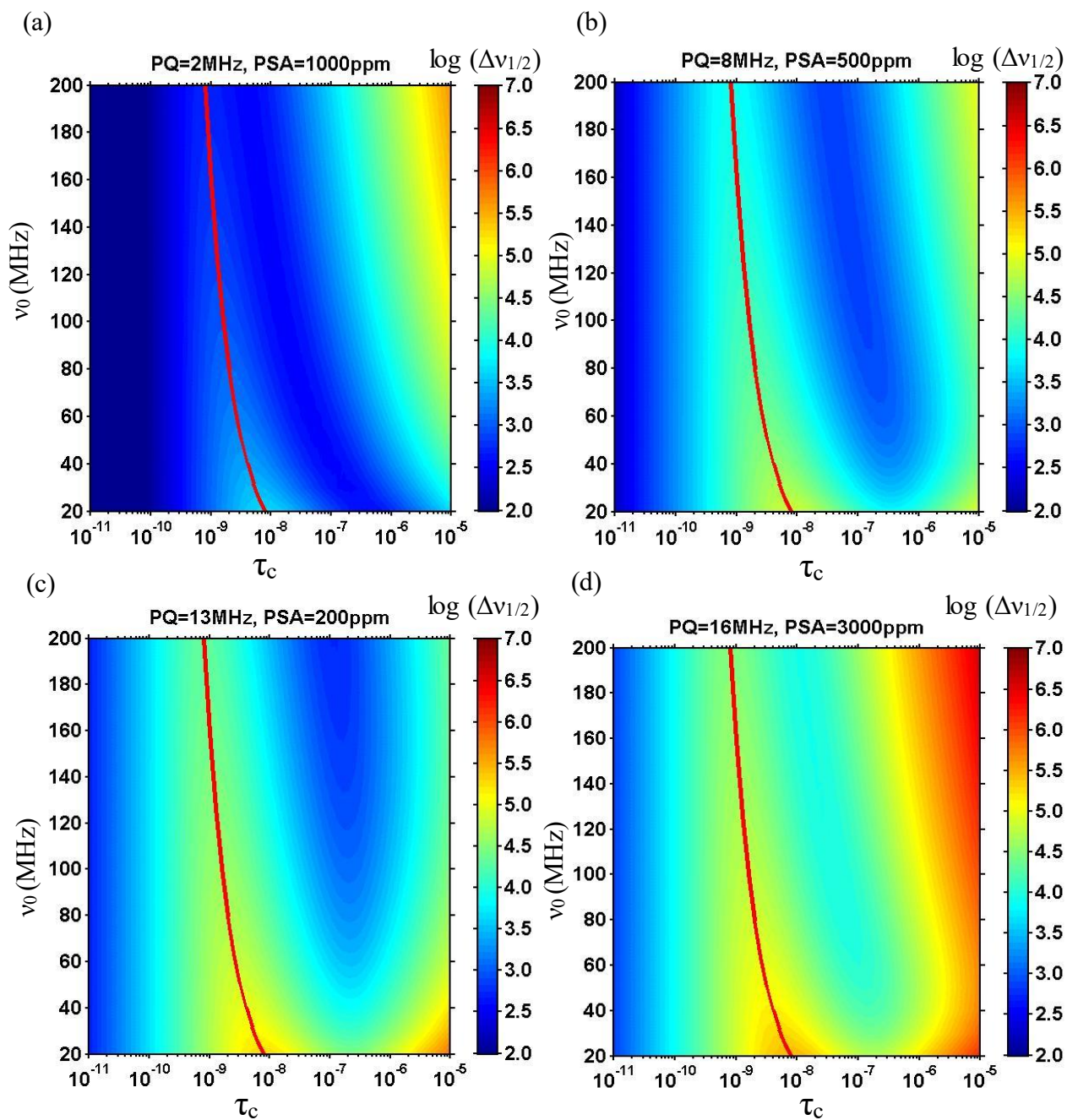
Figure 12. Illustration of the ^{17}O NMR line width, $\log(\Delta\nu_{1/2})$, in the ν_0-τ_c space for four typical combinations of P_Q and P_{SA}. The solid line indicates $\omega_0\tau_c = 1$. The line width along the z axis were calculated from eq. (23).

25

Chapter 3   QCT NMR Studies of Biologically Important Molecules

3.1   QCT ^{17}O NMR of Glucose

3.1.1   Introduction

Oxygen-17 has a nucleus of spin 5/2 with an extremely low natural abundance of 0.037%. One of the main reasons to study oxygen is its ubiquity in biological systems. Oxygen controls or participates in nearly every biological process and it occupies a key position both at the structural and at the physical level. Oxygen plays a major role in the molecular conformation of all biological macromolecules including peptides, proteins, DNA and RNA. For example, protein molecules are mostly stabilized by hydrogen bonds of the N-H···O type. Hence it is apparent that ^{17}O NMR will be an important probe to study the structure and function of these biological molecules. However, ^{17}O NMR studies are far less common than ^{1}H, ^{13}C and ^{15}N nuclei. This is because the quadrupolar nature of ^{17}O often results in broad signals in ^{17}O NMR spectra for solution samples. As a result, the conventional approach is to use solid-state NMR techniques. In the last several decades, solid-state ^{17}O NMR has been used to study a wide range of materials ranging from amorphous materials,[34] zeolites[35] and minerals[36] to polymers.[37] Apart from that, organic and biological molecules have also been studied by solid-state ^{17}O NMR.[38,39] However, solution-state NMR is still highly desirable for quadrupolar nuclei as it provides direct molecular structure information in solution especially for biological molecules. Recently, QCT ^{17}O NMR has been shown to be a new way of studying biological macromolecules in the solution state.[15,17,18,20] One of the objectives of this thesis is to further develop this new technique. In this section, we report on the synthesis and QCT ^{17}O NMR studies of glucose for which ^{17}O-labels are introduced at the 5- and 6-positions respectively: D-[5-^{17}O]-glucose and D-[6-^{17}O]-glucose (Fig. 13).

Figure 13. Molecular structures of (a) D-[5-^{17}O]-glucose and (b) D-[6-^{17}O]-glucose.

Glucose, the simplest form of sugar, plays an important role in human metabolism to maintain our living state. Glucose often comes from the breakdown of the food that human consumed and is absorbed into the bloodstream. It is an important energy source needed by all the cells and organs of our bodies. For example, brain and muscles both need glucose in order to function properly. Too much glucose in the bloodstream, however, can also bring health problems such as type II diabetes. Due to all those important roles that glucose plays in our body, it is quite necessary to develop ^{17}O NMR as a direct probe to study its functions and metabolisms in biological systems.

3.1.2 Experimental

3.1.2.1 Synthesis of D-[5-^{17}O]-Glucose

D-[5-^{17}O]-glucose was synthesized in four steps as illustrated in Fig. 14. First, 1,2-O-isopropylidene-D-glucofuranurono-6, 3-lactone (I) was oxidized to 1, 2-O-isopropylidene-D-xylo-hexofuranurono-6, 3-lactone-5-ulose hydrate (II) with a literature procedure.[33] Second, the ^{17}O labels were introduced to II to form [5,5-^{17}O$_2$]-II via an equilibrium process between the 5-keto and 5,5-gem-diol derivatives in methanol/H$_2$^{17}O.[40] Third, [5,5-^{17}O$_2$]-II was reduced with NaBH$_4$ to 1, 2-O-isopropylidene-[5-^{17}O]-α-D-glucofuranose (III).[41] Forth, removal of the protecting group led to the formation of D-[5-^{17}O]-glucose (IV).[42] The synthetic details are given below.

27
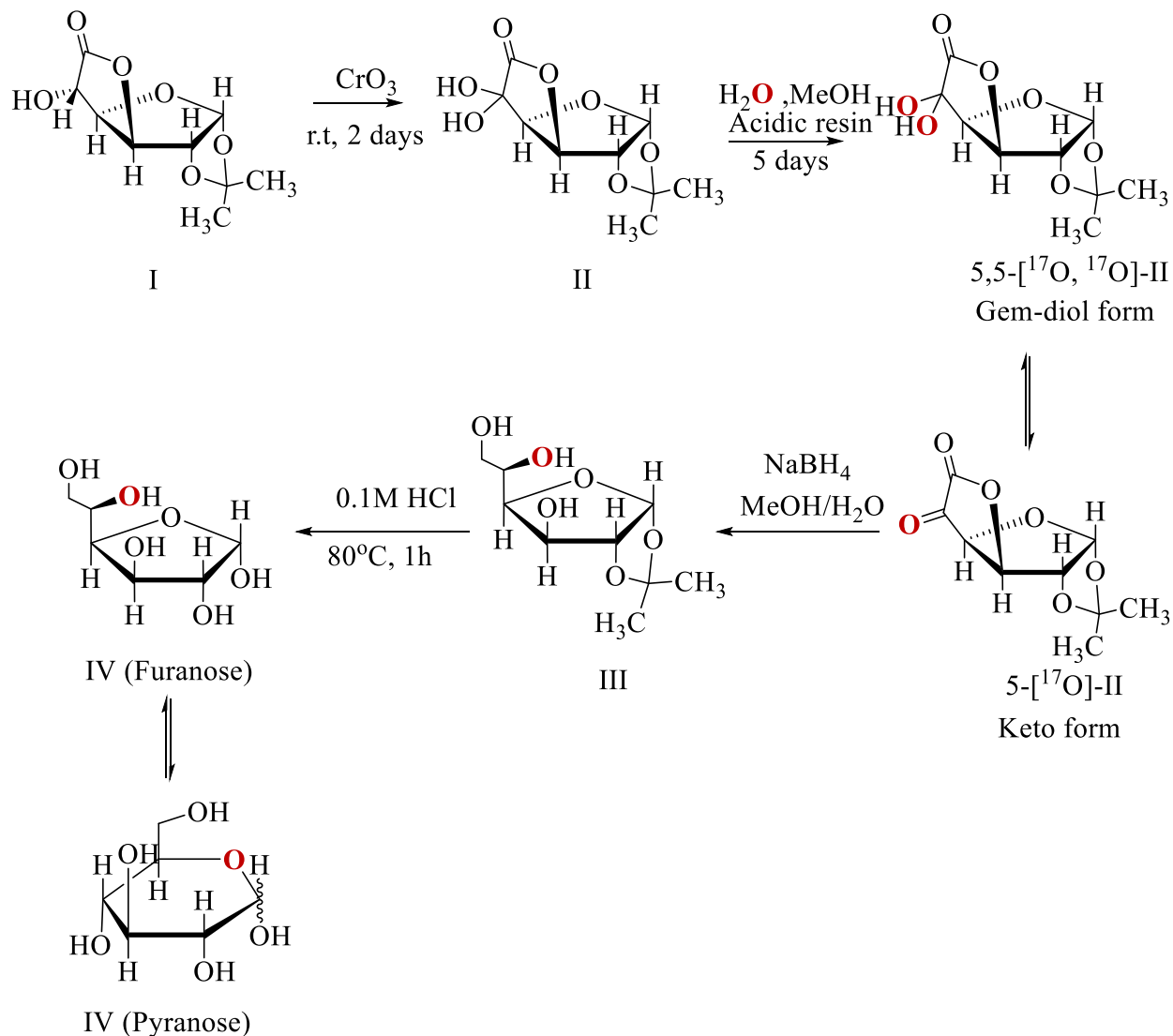
Figure 14. Synthetic pathways for the preparation of D-[5-^{17}O]-glucose.

Step 1: Preparation of 1,2-O-isopropylidene-D-xylo-hexofuranurono-6,3-lactone-5-ulose hydrate (II)[33]

CrO$_3$ (3.5 g, 35 mmol, Sigma Aldrich) was slowly added over 10 minutes to a solution of 1, 2-O-isopropylidene-D-glucofuranurono-6, 3-lactone (I) (3.8 g, 18 mmol, Alfa Aesar) in ethyl acetate (50 mL) under stirring. The dark red solution was stirred at room temperature for two days to result in a black slurry reaction mixture. The reaction mixture was filtered under vacuum and

the black cake was further washed with hot ethyl acetate (15 mL). After decoloring with activated carbon, the clear filtrate was evaporated to dryness. The white solid was dissolved in ethyl acetate (30 mL) and then hexane (10 mL) was added to precipitate white solid II (4.0 g, 98%). ^{1}H NMR (300 MHz, DMSO-d_6, δ): 7.45 and 7.28 (s, *gem*-OH), 5.92 (H-1, d, $J_{1,2}$ = 3.5 Hz,1H), 4.79 (H-2, d, J_{1-2} = 3.5 Hz, 1H), 1.39 (s, 3H), 1.24 (s, 3H), 4.82(H-3, d, $J_{3,4}$ = 2.8 Hz, 1H), 4.36 (H-4, d, $J_{3,4}$ = 2.8 Hz, 1H). ^{13}C NMR (75.0 MHz, DMSO-d_6, δ): 172.79, 112.51, 106.73, 93.60, 82.34, 82.18, 82.11, 27.16, and 26.83 ppm.

Step 2: Preparation of ([5,5-[17]O_2]-II)[40]

1,2-O-isopropylidene-D-xylo-hexofuranurono-6,3-lactone-5-ulose hydrate (II) (220 mg, 0.950 mmol) was dissolved in 8 mL methanol and 160 μL H_2[17]O (40% [17]O atom, purchased from CortecNet), to which 5 grains of Amberlite-IR 120 (H^+) resins were added. The solution was allowed to stand at room temperature for 5 days, during which ^{17}O NMR was used periodically to monitor the equilibrium process. ^{17}O NMR (67.7 MHz, methanol-d_4, δ): 60, 45, 0 ppm (water) and -24 ppm (MeOD).

Step 3: Preparation of 1,2-O-isopropylidene-α-D-[5-[17]O]-glucofuranose (III)[41]

To a solution of [5,5-[17]O_2]-II (220 mg, 0.950 mmol) in 8 mL methanol (directly from Step 2), a solution of sodium borohydride (150 mg, 3.96 mmol, Sigma Aldrich) in methanol (5 mL) was added dropwise. After 40 min, the solution was neutralized with Amberlite-IR 120 (H^+). The residue was treated several times with methanol to remove borate. The white solid (190 mg) was then further recrystallized from ethyl acetate to give III (103 mg, 49%). The ^{1}H NMR data shown below confirm that III is the gluco epimer. ^{1}H NMR (600 MHz, methanol-d_4, δ): 5.85 (H-1,d, $J_{1,2}$

= 3.6 Hz, 1H), 4.46 (H-2, dd, $J_{1,2}$ = 3.6 Hz, $J_{2,3}$ < 0.1Hz, 1H), 4.19 (H-3, dd, $J_{3,4}$ = 2,62 Hz, $J_{2,3}$ <

0.1 Hz, 1H), 3.99 (H-4, dd, $J_{3,4}$ = 2.62 Hz, $J_{4,5}$ = 8.38 Hz, 1H), 3.87 (H-5, ddd, $J_{4,5}$ = 8.38 Hz, $J_{5,6b}$

= 6.0 Hz, $J_{5,6a}$ = 3.16 Hz, 1H), 3.74 (H-6a, dd, $J_{5,6a}$ = 3.16 Hz, $J_{6a,6b}$ = 11.53 Hz, 1H), 3.57 (H-6b,dd,

$J_{5,6b}$ = 6.0 Hz, $J_{6a,6b}$ = 11.53 Hz, 1H); ^{13}C NMR(150 MHz, methanol-d_4, δ): 112.67, 106.33, 86.50,

81.28, 75.35, 70.34, 65.13, 26.99, 26.28 ppm. ^{17}O NMR (81.4 MHz, methanol-d_4, δ): δ = 4, -37

ppm (MeOD).

Step 4: D-[5-^{17}O]-glucose (IV)[42]

A mixture of 1,2-O-isopropylidene-α-D-[5-^{17}O] glucofuranose (III) (103 mg, 0.470 mmol)

and 4 mL of 0.1 M HCl was heated at 80 °C for 1 h. The solution was then neutralized with NaOH

(aq). The solution was evaporated to dryness to give white solid IV (84.0 mg). Note that the solid

so obtained is a D-[5-^{17}O]-glucose/NaCl complex. The level of ^{17}O enrichment in IV was estimated

to be 10% by solution ^{17}O NMR. ^{1}H NMR (300 MHz, D$_2$O, δ): 5.32 (αH-1), 4.74 (βH-1), multiple

peaks from 3.5-4 ppm. ^{13}C NMR (75.0 MHz, D$_2$O, δ): δ = 96.05 (αH-1), 92.18 (βH-1), 75.89,

75.70, 74.08, 72.72, 71.40, 69.58, 60.72, 60.56 ppm. ^{17}O NMR (67.7 MHz, D$_2$O, δ): δ = 65, 0 ppm

(D$_2$O).

3.1.2.2 Synthesis of D-[6-^{17}O]-glucose

D-[6-^{17}O]-glucose was synthesized in three steps as explained in Fig. 15. First, the ^{17}O

labels were introduced through Mitsunobu Reaction, converting the primary alcohol on 1,2-O-

isopropylidene-α-D-glucofuranose (V) into [^{17}O]-benzoyl group using Bz^{17}OH.[43] Second, 1,2-O-

isopropylidene-α-D-[6-^{17}O] glucofuranose (VII) was hydrolyzed back to primary alcohol under

basic condition.[43] Third, removal of the protecting group led to the formation of D-[6-^{17}O]-glucose

(IV).[42] The synthetic details are given below.
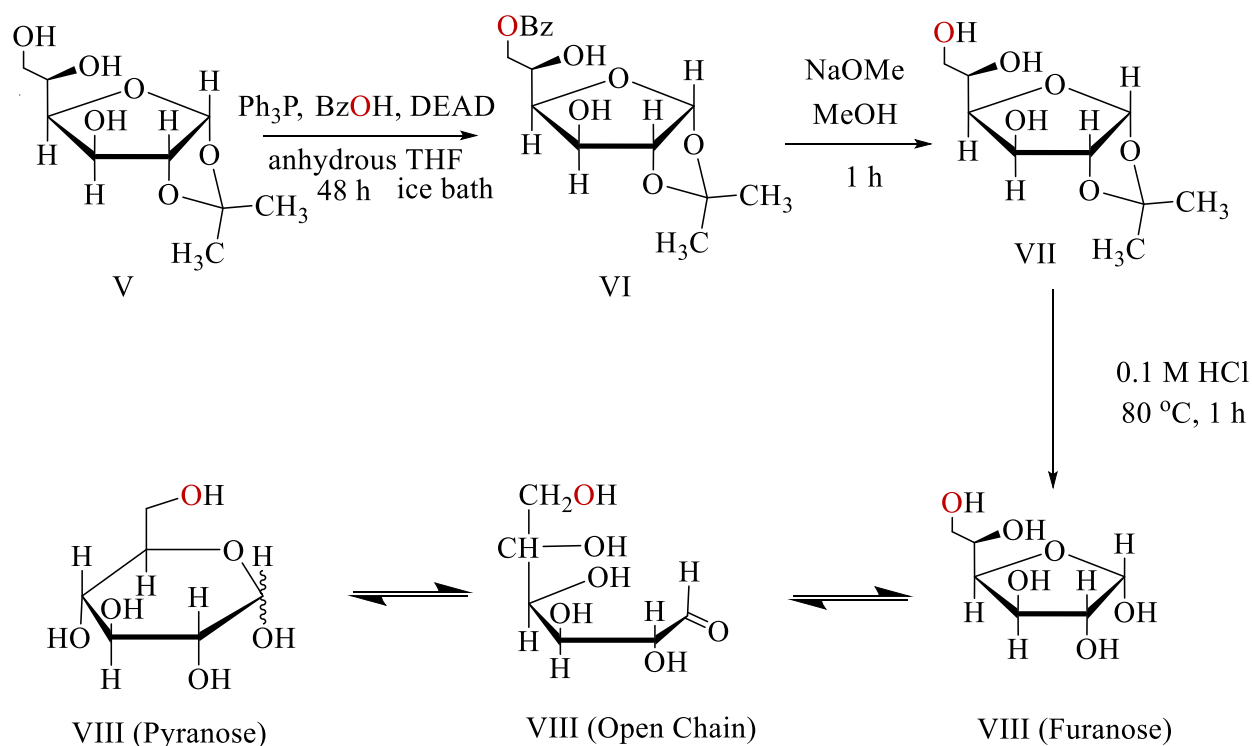
Figure 15. Synthetic pathways for the preparation of D-[6-^{17}O]-glucose.

Step 1: Preparation of [6-^{17}O]-Benzoyl-1,2-O-isopropylidene-α-D-glucofuranose (VI)[43]

In a 100 mL flask added with 1, 2-O-isopropylidene-α-D-glucofuranose (V) (330 mg, 1.50 mmol, Sigma Aldrich) and 24 mL anhydrous THF. After fully dissolved, ^{17}O labelled BzOH (193 mg, 1.58 mmol), PPh$_3$ (786 mg, 3.00 mmol, Sigma-Aldrich) was added. Then it was treated with Diethyl azodicarboxylate (0.480 mL, 3.00 mmol, Alfa Aesar) dropwise in 0 °C with ice-water bath. The mixture was then stirred for 48 h at room temperature. TLC plate analysis [5:95, (v/v) MeOH/CH$_2$Cl$_2$] showed the reaction was complete. The mixture was evaporated and the crude residue was purified by column chromatography (9:91 (v/v) MeOH/CH$_2$Cl$_2$) to afford the white

solid VI (400 mg, 82%). ^{1}H NMR (300 MHz, DMSO –d_6, δ): 7.51-8.08 (m, 5H, Ar-H), 5.82 (H-1, d, 1H, $J_{1,2}$ = 3.6 Hz), 5.32 (OH, d, 1H, J = 5.0 Hz), 5.23 (OH, d, 1H, J = 5.7 Hz), 4.47 (H-6, dd, 1H, $J_{5,6}$ = 1.9 Hz, $J_{6,6'}$ = 11.3 Hz), 4.42 (H-2, d, 1H), 4.20 (H-6', dd, 1H, $J_{5,6'}$ = 5.5 Hz, $J_{6,6'}$ = 11.3 Hz), 4.09 (H-4, dd, 1H, $J_{3,4}$ = 2.3 Hz, $J_{4,5}$ = 4.9 Hz), 4.04 (H-5, m, 1H), 4.02(H-3, d, 1H), 1.37 (s, 3H, CH_3), 1.27 (s, 3H, CH_3).

Step 2: Preparation of 1, 2-O-Isopropylidene-α-D-[6-[17]O] glucofuranose (VII)[43]

A solution of sodium hydroxide in MeOH (~ 0.5 M, ~4 mL) was added to [6-[17]O]-Benzoyl-1, 2-O-isopropylidene-α-D-glucofuranose (VI) (400 mg, directly from step 1). The mixture was stirred for 1 h until it was shown by TLC analysis [5:95, (v/v) MeOH/CH_2Cl_2] that the reaction was complete. After that, the reaction mixture was neutralized by about 3 mL Amberlite H^{+} (1.8 meq/mL) and was filtered and concentrated. Later the residue was purified by another column chromatography [7:93, (v/v) MeOH/CH_2Cl_2] to give the white solid product VII (257 mg, 94%). ^{1}H NMR (600 MHz, methanol-d_4, δ): 5.87 (H-1, d, $J_{1,2}$ = 3.6 Hz, 1H), 4.48 (H-2, dd, $J_{1,2}$ = 3.6 Hz, $J_{2,3}$<0.1Hz, 1H), 4.21 (H-3, dd, $J_{3,4}$ = 2,62 Hz, $J_{2,3}$ < 0.1 Hz, 1H), 3.90 (H-4, dd, $J_{3,4}$ = 2.62 Hz, $J_{4,5}$ = 8.38 Hz, 1H), 3.75 (H-5, ddd, $J_{4,5}$ = 8.38 Hz, $J_{5,6b}$ = 6.0 Hz, $J_{5,6a}$ = 3.16 Hz, 1H), 3.61 (H-6a, dd, $J_{5,6a}$ = 3.16 Hz, $J_{6a,6b}$ = 11.53 Hz, 1H), 3.57 (H-6b, dd, $J_{5,6b}$ = 6.0 Hz, $J_{6a,6b}$ = 11.53 Hz, 1H); ^{13}C NMR (150 MHz, methanol-d_4, δ): 112.67, 106.33, 86.50, 81.28, 75.35, 70.34, 65.13, 26.99, 26.28 ppm. ^{17}O NMR (81.4 MHz, methanol-d_4, δ): δ = -16 ppm, -37 ppm (MeOD).

Step 3: Preparation of D-[6-[17]O]-glucose (VIII)[42]

A mixture of 1, 2-O-isopropylidene-α-D-[6-[17]O] glucofuranose (VII) (257 mg, 1.17 mmol) and 5 mL of 0.1 M HCl was heated at 80°C for 1 h. The solution was then neutralized with NaOH

(aq). The solution was evaporated to dryness to give white solid VIII (161 mg). Note that the solid obtained is a D-[6-^{17}O]-glucose/NaCl complex. ^{1}H NMR (300 MHz, D$_2$O, δ): 5.32 (αH-1), 4.74 (βH-1), multiple peaks from 3.5-4 ppm. ^{13}C NMR (75.0 MHz, D$_2$O, δ): δ = 96.05 (αH-1), 92.18 (βH-1), 75.89, 75.70, 74.08, 72.72, 71.40, 69.58, 60.72, 60.56 ppm. ^{17}O NMR (67.7 MHz, D$_2$O, δ): δ = -7, 0 ppm (D$_2$O).

3.1.2.3 NMR Experiments

All ^{17}O NMR experiments were performed on Bruker Avance-400, -500, -600 and -900 MHz spectrometers. Normally solution samples were prepared in 5-mm NMR tubes and Bruker broadband solution probes were used to record the NMR spectra. At 21.1 T, a 4-mm Bruker MAS probe was used. All ^{17}O chemical shifts were referenced to liquid water. All experiments at 21.1 T were performed by Dr. Victor Terskikh at the National Ultrahigh-field NMR Facility for Solids (Ottawa, Ontario, Canada). The effective 90°C pulse width of QCT ^{17}O NMR is 4.7 μs on Bruker Avance-400 and 7.0 μs on Bruker Avance-500, 600 MHz spectrometers.

3.1.3   Results and Discussion

Both D-[5-^{17}O]-glucose and D-[6-^{17}O]-glucose were dissolved in aqueous and glycerol solutions separately so that the molecular rotational correlation time (τ$_c$) of glucose can be controlled to cover a wide range (from the extreme narrowing to slow motion conditions). Fig. 16 shows the ^{17}O NMR spectra of D-[5-^{17}O]-glucose and D-[6-^{17}O]-glucose in these solutions obtained at different temperatures and at different magnetic fields. As shown in Fig. 16 (a) and (d), the ^{17}O NMR signals observed for D-[5-^{17}O]-glucose and D-[6-^{17}O]-glucose in water were found to be 65 ppm and -7 ppm, respectively, which are consistent with the literature.[44,45] The observed

^{17}O NMR line width of these signals decreases as the temperature of the sample increases. For example, the ^{17}O NMR line width of D-[5-[17]O]-glucose is reduced to only 0.79 kHz at 355 K from 2.10 kHz observed at 298 K; Fig. 16 (a). Similarly, the [17]O line width of D-[6-[17]O]-glucose changes from 1.01 kHz at 298 K to only 0.45 kHz at 355 K; Fig. 16 (d). These observations suggest that glucose is in the fast motion regime under these conditions ($\omega_0 \tau_c \ll 1$).
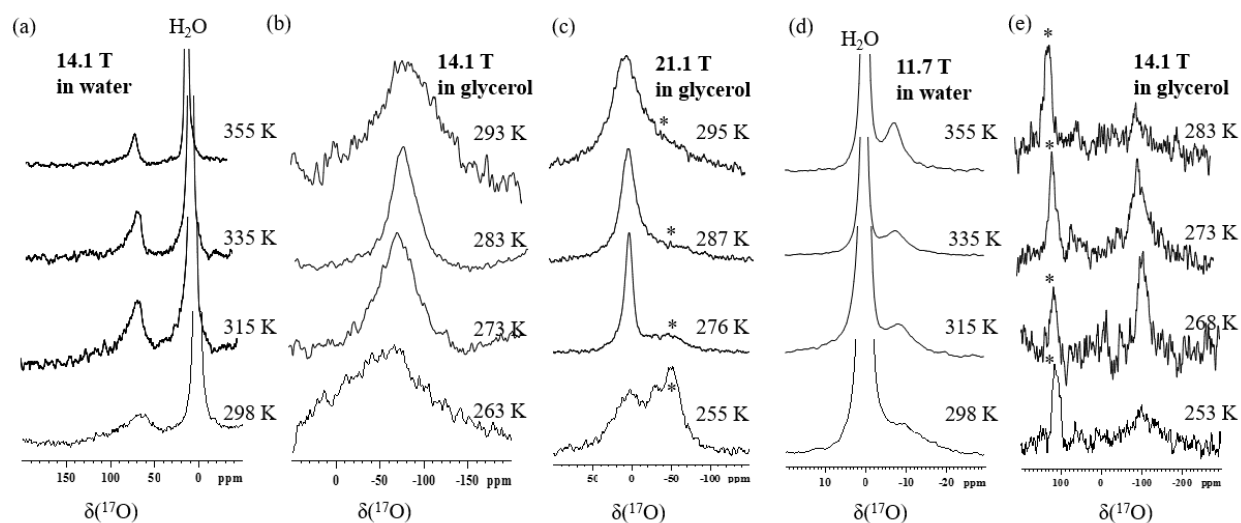
Figure 16. VT ^{17}O NMR spectra of D-[5-[17]O]-glucose and D-[6-[17]O]-glucose in aqueous and glycerol solutions. (a) 35 mg D-[5-[17]O]-glucose in 0.6 mL D$_2$O. (b) and (c) 22 mg D-[5-[17]O]-glucose in 0.268 g of glycerol. (d) 29 mg of D-[6-[17]O]-glucose in 0.6 mL D$_2$O. (e) 40 mg of D-[6-[17]O]-glucose in 0.420 g glycerol. Natural abundance ^{17}O NMR signals from glycerol (~ -40 ppm) are marked with * in (c) and the signal from the glass tube (~120 ppm) are marked with * in (e).

When glucose is dissolved in glycerol, a very viscous solvent, the molecular rotational correlation time of glucose can increase significantly as compared with that in aqueous solution at the same temperature. Now as seen in Fig. 16 (b) (c) and (e), the observed ^{17}O NMR signals D-[5-[17]O]-glucose and D-[6-[17]O]-glucose are all significantly shifted to lower frequencies from their respective chemical shifts, 65 and -7 ppm. For example, in Fig. 16 (b) and (e), at 14.1 T, the [17]O CT signal of D-[5-[17]O]-glucose appears at -74 ppm, and the [17]O CT signal of D-[6-[17]O]-glucose appears at -100 ppm. Both of the chemical shifts were significantly shifted due to the dynamic

34

frequency shift for the CT.[46] In addition, only the CT was observed, suggesting that glucose molecules are already in the slow motion regime ($\omega_0 \tau_c \gg 1$) at all the temperatures employed, as explained in Section 2.1. Interestingly, the line width of the CT signal of D-[5-^{17}O]-glucose decreases with the sample temperature, reaches a minimum of about 2.50 kHz at 273 K. The ^{17}O CT signal of D-[6-^{17}O]-glucose displays a similar trend. These observations can be explained from eq. (23). For the Q term, the line width decreases with the increase of τ_c while Q2 and SA terms both increase with τ_c. Hence it can be deduced that the quadrupole interaction (Q) is the dominating relaxation mechanism for the CT at these temperatures. Below 273 K for D-[5-^{17}O]-glucose and 268 K for D-[6-^{17}O]-glucose at 14.1 T, which is the so called ultraslow motion range ($1 \ll \omega_0 \tau_c < (\omega_Q \tau_c)^2$), where ω_Q is the nuclear quadrupole coupling constant in angular frequency unit (i.e., $\omega_Q = 2\pi C_Q$), the ^{17}O line width begins to increase with the decrease of sample temperature, suggesting that now the dominating relaxation mechanisms for the CT should be the second-order quadrupole interaction and the shielding anisotropy as both of them are proportional to τ_c.

The ^{17}O CT signal observed at 21.1 T for D-[5-^{17}O]-glucose, shown in Fig. 16 (c), displays essentially the same temperature dependence. However, two spectral features are worth noting. First, the ^{17}O CT signal now appears at 5 ppm. Secondly, the minimum line width of D-[5-^{17}O]-glucose observed at 276 K is only 1.46 kHz, which is considerably smaller than that observed at 14.1 T, which is 2.50 kHz. Because from eq. (23), the Q2 term is proportional to $(1/\nu_0)^2$ while the SA term is proportional to $(\nu_0)^2$, the diminution of the line width with the increase of the magnetic field clearly suggests the Q2 term is dominant for glucose. The CT nature of the ^{17}O NMR signals for glucose in glycerol is further confirmed by examining the signal positions at multiple magnetic fields. As illustrated in Fig. 17, the observed signal positions (in ppm) vary linearly with $(1/\nu_0)^2$ as expected from eq. (31).[46] For D-[5-^{17}O]-glucose, the slope of the solid line shown in Fig. 17 yields

35

a P_Q value of 12.4 MHz and the y- intercept of the line is 66 ppm, which is in excellent agreement with the isotropic ^{17}O chemical shift observed for D-[5-^{17}O]-glucose in aqueous solution where glucose is in the fast motion regime. Similarly, we obtained a P_Q value of 10.2 MHz and chemical shift of -8 ppm for D-[6-^{17}O]-glucose.
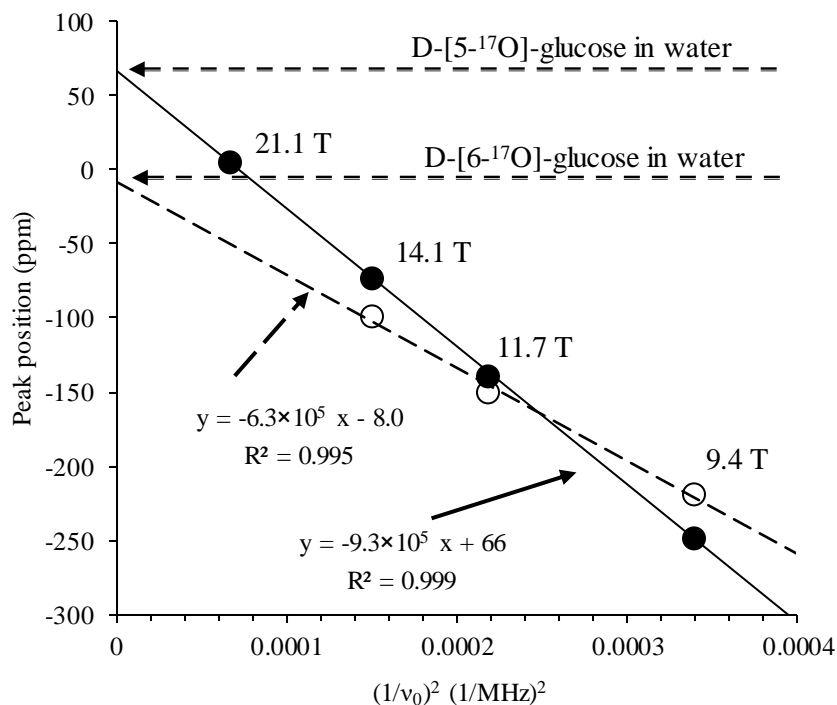
Figure 17. Observed ^{17}O NMR peak positions for D-[5-^{17}O]-glucose (closed circles) and D-[6-^{17}O]-glucose (open circles) in glycerol at different magnetic fields.

Table 2 summarizes the experimental data of D-[5-^{17}O]-glucose and D-[6-^{17}O]-glucose in aqueous solution and glycerol at different magnetic fields. To quantitatively analyze the ^{17}O line width (or transverse relaxation rate) data obtained for D-[5-^{17}O]-glucose and D-[6-^{17}O]-glucose in two solvents over the entire temperature range (253 K to 355 K), τ_c at different temperatures were determined using the SED model according to eq. (9). The viscosity of water at different temperatures were obtained from the literature,[47] and the viscosity in glycerol were calculated

based on the following equation from the literature:[48]

$$\eta = \eta^{o}\exp\left[(28.75 - \ln\eta^{o})\left(\frac{T_g}{T}\right)^{\alpha}\right] \tag{33}$$

where the viscosity is measured in Pa·s, and $\eta^{o} = 6.3 \cdot 10^{-4}$ Pa·s, $T_g = 177$ K, and $\alpha = 3.2$. It can be seen from Table 2 that by using two different solvents at different temperatures, the motion of glucose can span over 6 orders of magnitude, from extreme narrowing ($\omega_0\tau_c = 3.47 \times 10^{-3}$) to ultraslow motion ($\omega_0\tau_c = 1862$).

Table 2. Solvent viscosity, molecular rotational correlation time, and ^{17}O NMR line width for D-[5-^{17}O]-glucose and D-[6-^{17}O]-glucose at multiple magnetic fields in aqueous and glycerol solutions.

D-[5-^{17}O]-glucose							D-[6-^{17}O]-glucose		
In glycerol			14.1 T		21.1 T			14.1 T	
Temp (K)	η (Pa·s)	τ_c (ns)	$\omega_0\tau_c$	$\Delta\nu_{1/2}$ (kHz)	$\omega_0\tau_c$	$\Delta\nu_{1/2}$ (kHz)	τ_c (ns)	$\omega_0\tau_c$	$\Delta\nu_{1/2}$ (kHz)
253	63.1	3360	1718	7.80			2030	1039	6.23
255	47.4	2430			1862	5.49			
263	16.5	826	421	5.40	633	2.66	246	126	3.03
269	8.12	401			307	1.83	156	79.9	2.03
273	5.24	256	131	2.50			113	58.0	2.93
276	3.85	183			140	1.46			
281	2.36	111			85.1	1.59			
283	1.97	92.3	47.2	3.80			39.2	20.0	5.55
287	1.38	63.5			48.7	2.68			
293	0.843	38.5	19.7	6.80					
295	0.720	32.1			24.6	5.12			
303	0.405	17.7	9.06	9.40					
In water			14.1 T					14.1 T	
Temp (K)	η (mPa·s)	τ_c (ps)	$10^3\omega_0\tau_c$	$\Delta\nu_{1/2}$ (kHz)			τ_c (ps)	$10^3\omega_0\tau_c$	$\Delta\nu_{1/2}$ (kHz)
298	0.89	40.3	20.6	2.10			24.3	10.3	1.01
303	0.797	35.5	18.1	2.00			21.4	9.11	0.82
315	0.653	28.1	14.4	1.40			17.0	7.22	0.68
325	0.547	22.8	11.7	1.26			13.8	5.86	0.63
335	0.466	18.9	9.64	1.08			11.4	4.84	0.54
345	0.404	15.9	8.10	0.90			9.58	4.07	0.53
355	0.354	13.5	6.91	0.79			8.17	3.47	0.45

* The uncertainty in $\Delta\nu_{1/2}$ is $\pm$ 0.01 kHz.

Fig. 18 (a) shows the experimental VT ^{17}O NMR data obtained for D-[5-^{17}O]-glucose and D-[6-^{17}O]-glucose in both water and glycerol. The theoretical curves were calculated from eq. (23). A simultaneous fit of the line width data collected at two magnetic fields produced the following parameters for D-[5-^{17}O]-glucose: V_h = 186 ± 10 Å^3 (r = 3.7 Å for a spherical model), P_Q = 14.5 MHz, P_{SA} = 250 ppm. The V_h value for D-[5-^{17}O]-glucose compares well with the molecular volume calculated from the crystal density, 193 Å^3, as well as the partial molecular volume, 186 Å^3, determined for D-glucose in aqueous solution.[49] The P_Q values obtained from the line width analysis shown in Fig. 18 (a) are also in reasonable agreement with that determined from the dynamic frequency shifts discussed earlier.
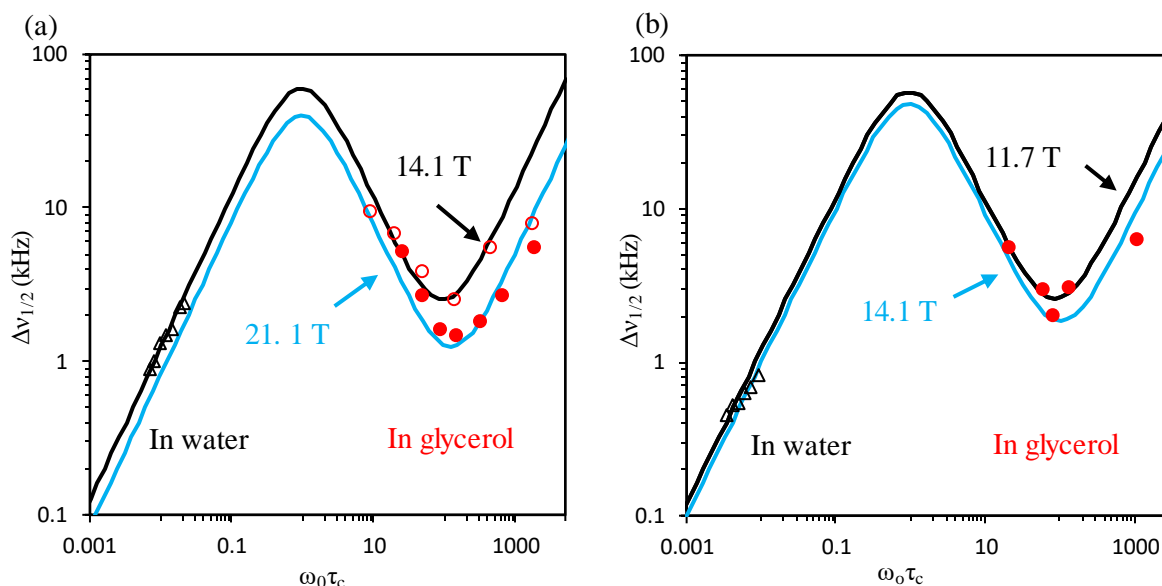
Figure 18. Experimental ^{17}O NMR line width for (a) D-[5-^{17}O]-glucose and (b) D-[6-^{17}O]-glucose in water and in glycerol solutions at different frequencies. All the theoretical curves were calculated based on eq. (23) with the parameters given in the text.

For D-[6-^{17}O]-glucose data shown in Fig. 18 (b), the parameters obtained from a similar analysis were: V_h = 112 ± 10 Å^3 (r = 3 Å for a spherical model), P_Q = 13.0 MHz, P_{SA} = 250 ppm. P_Q value is consistent with that determined earlier in Fig. 17. However, the present hydrodynamic

volume obtained does not show full agreement with that obtained using D-[5-^{17}O]-glucose. This is because the fitting was only based on the data collected at 11.7 T and 14.1 T, there might be some experimental error arisen from it, suggesting line width measurements at higher frequencies (i.e. at 21.1 T) are needed to better fit the curve and thus more accurate parameters to be obtained.

3.1.4 Conclusions

We have shown in this section that at slow motion, the quadrupolar interaction dominates the CT ^{17}O signal for glucose. Under the ultraslow motion condition, the second-order quadrupolar interaction, instead of the shielding anisotropy, becomes a predominant nuclear spin relaxation mechanism for the CT ^{17}O signal in glucose. While this phenomenon was predicted by theory several decades ago, the present study represents the first experimental observation of this rather unusual situation. This new relaxation mechanism is an important contributor to the resolution limit in QCT NMR. We have also shown that P_Q, P_{SA} and hydrodynamic volume can be obtained simultaneously from ^{17}O QCT NMR studies of glucose in solution. This provides supplementary information for the NMR parameters of hydroxyl group in organic molecules.

3.2   QCT ^{17}O NMR of Nicotinamide

3.2.1   Introduction

Nicotinamide, also known as niacin amide or nicotinic amide, is the amide derivative of nicotinic acid (Vitamin B$_3$/Niacin). Nicotinamide is water-soluble vitamin belonging to the Vitamin B group. Nicotinamide is the biologically active form of nicotinic acid. It is mostly received in human bodies from two sources: firstly, in food such as various meat, peanuts, and sunflower seeds; secondly by converting tryptophan, an amino acid regularly found in the body, into niacin and then into nicotinamide. Nicotinamide is believed to improve energy production due to its role as a precursor of NAD (Nicotinamide Adenosine Dinucleotide) and Nicotinamide adenine dinucleotide phosphate (NADP), which are coenzymes in a wide variety of enzymatic oxidation-reduction reactions. Nicotinamide is also used as a medicine for skin treatment. For example, it has been reported to effectively treat acne vulgaris by its anti-inflammatory action and reducing sebum.[50] It can decrease water loss through the epidermis and thus increase skin hydration. It can also improve the complexion of aging skin. By reducing actinic keratosis, it can possibly reduce the risk of skin cancer.[51] In this work, the ^{17}O-labelled nicotinamide (Fig. 19) was studied by QCT ^{17}O NMR in order to determine its ^{17}O NMR parameters. Another important feature of nicotinamide is that the amide group can be used as a model for the peptide bond in proteins.
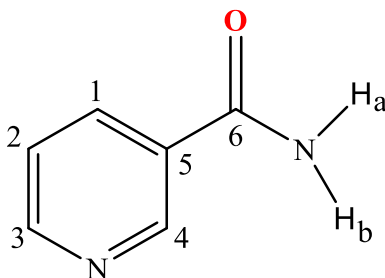
Figure 19. Molecular structure of [^{17}O]-nicotinamide.

3.2.2 Experimental

[^{17}O]-nicotinamide was synthesized by Dr. Xianqi Kong following a literature method.[52] All ^{17}O NMR experiments were performed on Bruker Avance-400, -500, -600 and -900 MHz spectrometers. Normally solution samples were prepared in 5-mm NMR tubes and Bruker broadband solution probes were used to record the NMR spectra. All ^{17}O chemical shifts were referenced to liquid water. All experiments at 21.1 T were performed by Dr. Victor Terskikh at the National Ultrahigh-field NMR Facility for Solids (Ottawa, Ontario, Canada).

3.2.3 Results and Discussion

[O^{17}]-nicotinamide was dissolved in glycerol and various temperature ^{17}O NMR experiments at multiple magnetic fields were conducted, as is shown in Fig. 20. At high temperature range (333-363 K), the molecular tumbling time is in the extreme narrowing range. For instance at 11.7 T, the ^{17}O isotropic chemical shift of [^{17}O]-nicotinamide was found to be 303 ppm. As expected, the observed ^{17}O line width decreases as the temperature of the sample increases. For example, the ^{17}O line width of [^{17}O]-nicotinamide of 7.60 kHz observed at 333 K was found to be 2.45 kHz at 363 K. At low temperatures (295-253 K), as shown in the rest spectra in Fig. 20, however, the molecular rotational correlation time of [^{17}O]-nicotinamide increases drastically. Now at 283 K, [^{17}O]-nicotinamide is already in the slow motion regime ($\omega_o \tau_c \gg 1$). As a result, only the ^{17}O CT signal was observed for [^{17}O]-nicotinamide in glycerol between 283 and 253 K at 9.4 T. The ^{17}O CT signal of [^{17}O]-nicotinamide at 148 ppm at 9.4 T is also considerably shifted from the true chemical shift, 303 ppm, due to the dynamic frequency shift for the CT.

At this slow motional range (283-253 K), the line width of the CT signal of [^{17}O]-nicotinamide shows the same temperature dependence as that of D-glucose in glycerol, as discussed in Section 3.1. It first decreases and then increases with the sample temperature at ultraslow motion range. For instance, at 11.7 T, the line width of [^{17}O]-nicotinamide decreases with the sample temperature until it reaches a minimum of about 1.80 kHz at 263 K. Interestingly, the line width is even narrower than that observed at 363 K, which is 2.45 kHz. This suggests that the QCT NMR technique can achieve much better resolution than regular NMR studies. In addition, low temperatures are preferable for biological molecules than high temperatures.
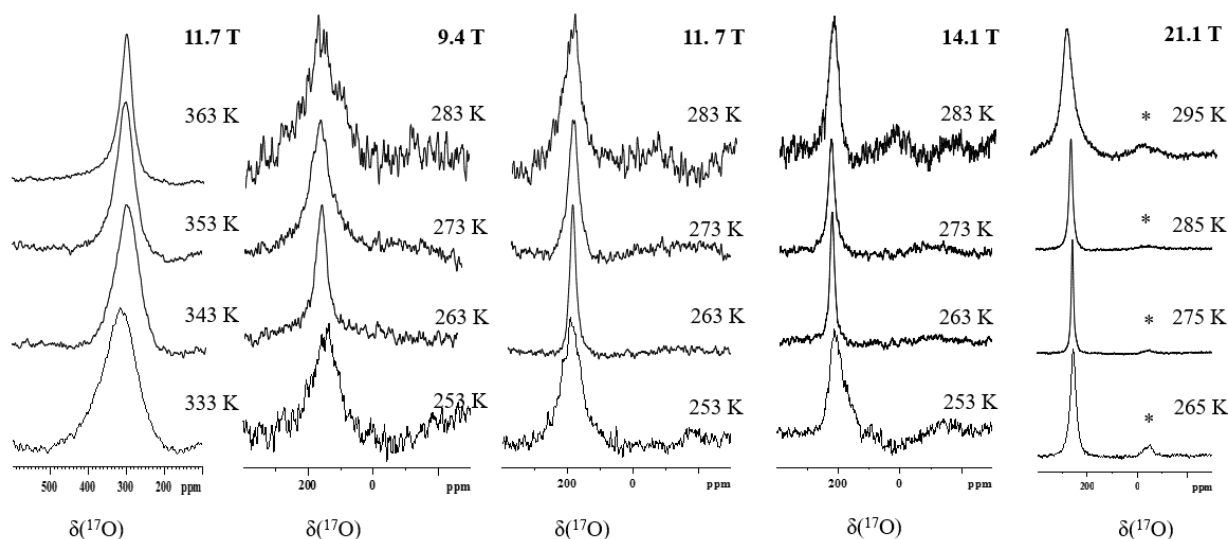
Figure 20. VT ^{17}O NMR spectra of 74 mg [10%-^{17}O]-nicotinamide in 0.567 g glycerol at various magnetic fields. The natural abundance ^{17}O NMR signals from glycerol (~ -50 ppm) are marked with *.

Since the overall line width decreases with the increase of τ_c from 283 K to 263 K, it can be deduced from eq. (23) that the quadrupole interaction (Q) is ruling the relaxation mechanism for the CT at this slow motion range ($1 \ll \omega_0\tau_c < \omega_Q\tau_c$), where ω_Q is the nuclear quadrupole coupling constant in angular frequency unit (i.e., $\omega_Q = 2\pi C_Q$). However, as $\omega_0\tau_c$ further increases

(i.e. the ultraslow motion), the line width begins to increase again with the decrease of temperature below 263 K, suggesting that now the relaxation mechanism for the CT is the second-order quadrupole interaction and the shielding anisotropy, as illustrated in Section 2.1.

By analyzing the [17]O CT signal line width of [[17]O]-nicotinamide at various magnetic fields (Fig. 20), it can be noted that the resolution is not greatly improved at high magnetic field like glucose does. For example, the minimum line width observed at 268 K is 1.29 kHz at 21.1 T, while the line width observed at 14.1 T is 1.40 kHz at 263 K. This suggests that the second order quadrupole interaction is no longer the dominant interaction at the ultraslow range, the shielding anisotropy also contribute a lot in this case, as the second order quadrupole is inversely proportional to v_0^2 and the shielding anisotropy is proportional to v_0^2, while v_0 is the Larmor frequency under detection.
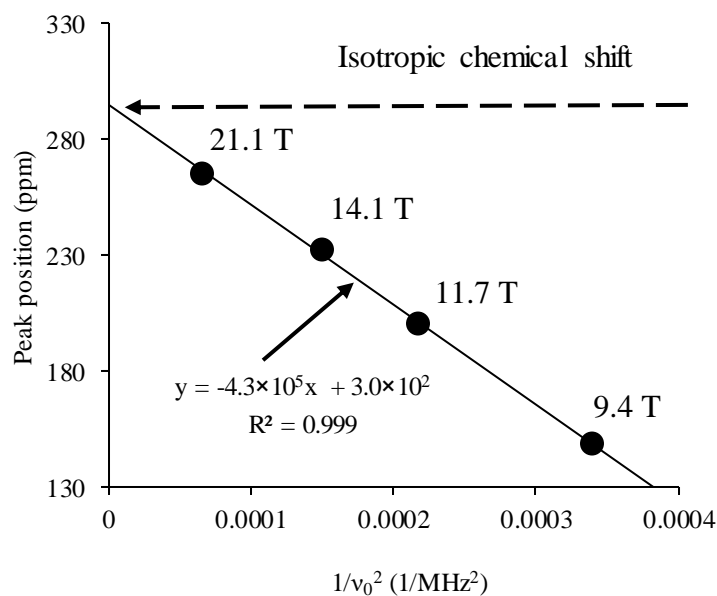
Figure 21. Observed ^{17}O NMR peak positions for [[17]O]-nicotinamide in glycerol at different magnetic fields.

The distinct feature of QCT NMR, which is the dynamic frequency shift effect, was also further investigated. Fig. 21 plots the observed signal position (in ppm) versus $(1/\nu_0)^2$. As expected from eq. (31), it shows a linear dependence. The chemical shift for [^{17}O]-nicotinamide are 148 ppm, 200 ppm and 232 ppm respectively at 9.4 T, 11.7 T and 14.1 T. The y-intercept shows the isotropic value of nicotinamide as 300 ppm, which corresponds well with the ^{17}O signal observed under extreme narrowing condition. The P_Q value was also obtained as 8.5 MHz using the slope of the figure, which is consistent with the literature values for the amide functional groups.[29,30]

Table 3. Solvent viscosity, molecular rotational correlation time, and ^{17}O NMR line width for [^{17}O]-nicotinamide in glycerol solutions at multiple magnetic fields.

At low temperatures			9.4 T		11.7 T		14.1 T		21.1 T	
Temp (K)	η (Pa·s)	τ_c (ns)	$\omega_0\tau_c$	$\Delta\nu_{1/2}$ (kHz)	$\omega_0\tau_c$	$\Delta\nu_{1/2}$ (kHz)	$\omega_0\tau_c$	$\Delta\nu_{1/2}$ (kHz)	$\omega_0\tau_c$	$\Delta\nu_{1/2}$ (kHz)
248	135	2370	806		1005	9.00	1208			
253	63.1	1090	370	5.10	461	4.60	554	4.00		
258	31.4	529	180	3.95	225	2.80	270	2.40	405	3.20
263	16.5	272	92.8	2.40	116	1.80	139	1.40	209	2.20
268	9.09	147	50.2	2.20	62.6	1.92	75.4	1.60	113	1.29
273	5.24	83.5	28.5	3.50	35.5	2.40	42.7	2.10	64	
278	3.15	49.3	16.8	5.80	20.9	3.50	25.2	2.70	37.8	1.40
283	1.97	30.2	10.3	6.80	12.8	5.10	15.4	4.60	23.1	2.00
288	1.27	19.1	6.52		8.13	6.10	9.78	5.70	14.7	
290	1.07	16.1	5.48		6.84		8.21		12.3	3.30
295	0.72	10.6	3.63		4.52		5.44		8.15	5.70

At high temperatures			11.7 T	
Temp (K)	η (mPa·s)	τ_c (ps)	$10^3\omega_0\tau_c$	$\Delta\nu_{1/2}$ (kHz)
318	160.4	512	217	11.55
323	122.5	385	163	10.25
328	95.13	294	125	8.55
333	75.04	229	97.2	7.60
338	60.07	180	76.6	6.00
343	48.73	144	61.2	4.60
348	40.02	117	49.6	3.90
353	33.26	95.6	40.6	3.50
358	27.93	79.1	33.6	3.05
363	23.69	66.2	28.1	2.45

* The uncertainty in $\Delta\nu_{1/2}$ is $\pm$ 0.01 kHz.

Table 3 shows the line width measurements of $[^{17}O]$-nicotinamide at various magnetic fields in glycerol solutions. The τ_c values were calculated from the modified SED model using eq. (10). As can be seen, the $[^{17}O]$-nicotinamide molecular motion coveres over 5 orders of magnitude from extremely narrowing ($\omega_0\tau_c = 0.0281$) to ultraslow motion regime ($\omega_0\tau_c = 1208$).
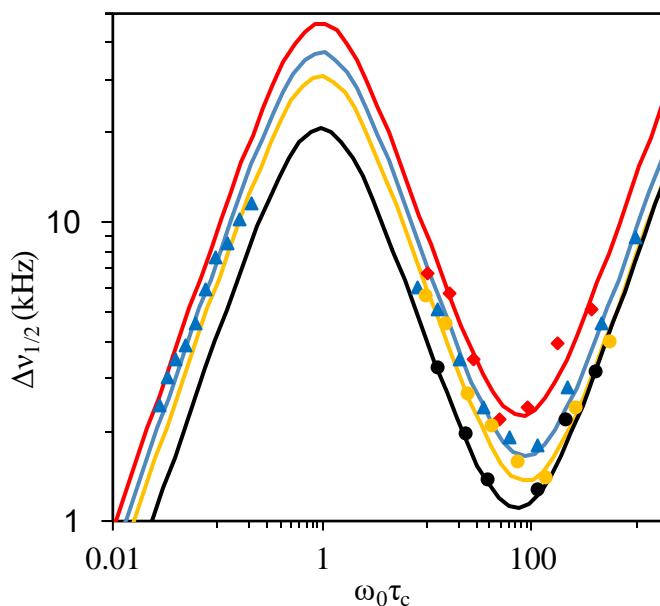
Figure 22. Experimental line width of $[^{17}O]$-nicotinamide in glycerol at 9.4 T (red squares), 11.7 T (blue triangles), 14.1 T (yellow circles) and 21.1 T (black circles), and corresponding theoretical curves calculated based on eq. (23) with the parameters given in the text.

To fit the calculated line width at different magnetic fields, a series of parameters were produced: $P_Q = 10.4$ MHz and $P_{SA} = 550$ ppm, as is displayed in Fig. 22. The P_Q and P_{SA} parameters compare well with the literature values for amides.[29,30] Since the P_{SA} term is now almost twice of that of glucose, it further confirms the previous observation in Fig. 20 that the shielding anisotropy contribution here is much significant than that for glucose. This suggests that for nicotinamide, the second-order quadrupole interaction and the shielding anisotropy contribution are comparable, which is different from glucose where the second-order quadrupole interaction dominates in this

region. This suggests there exists an optimal region to perform ^{17}O QCT NMR for amide group containing molecules, which is consistent with the plot shown in Fig. 12 (b) in section 2.3.

The effective volume in glycerol produced from fitting was $V_{effective} = 60$ Å^3 at low temperatures and $V_{effective} = 14$ Å^3 at high temperatures. Surprisingly, the volumes used were significant smaller than that calculated from crystal structure, which is 144 Å^3.[53] The discrepancy can be reasonably explained by the modified SED volume model.[21] By introducing the constant C, which is the boundary condition parameter dependent on the property of solute, solvent and concentration, as is discussed in section 1.3.3, it can be determined that the rotational dynamics of nicotinamide lies in the slip limit range since C is usually significantly smaller than 1 in this case. Hence, it is assumed that glycerol molecules do not rotate with nicotinamide molecules and the resistance only came from the displacement of some glycerol molecules as nicotinamide molecules rotate. In this case, $V_h \cdot C = 14$ Å^3 at high temperatures and $V_h \cdot C = 60$ Å^3 at low temperatures. The larger effective volume at low temperatures may be explained by the strong hydrogen bonding between nicotinamide molecules, which slows down the tumbling process. This hypothesis can be confirmed by doing ^1H NMR of nicotinamide at various temperatures. As is shown in Fig. 23, two protons on NH$_2$ group of nicotinamide were shifted to higher chemical shift at lower temperatures and to lower chemical shift at higher temperatures while other four normal protons did not shift, which suggests the stronger hydrogen bonding between NH groups at lower temperatures.
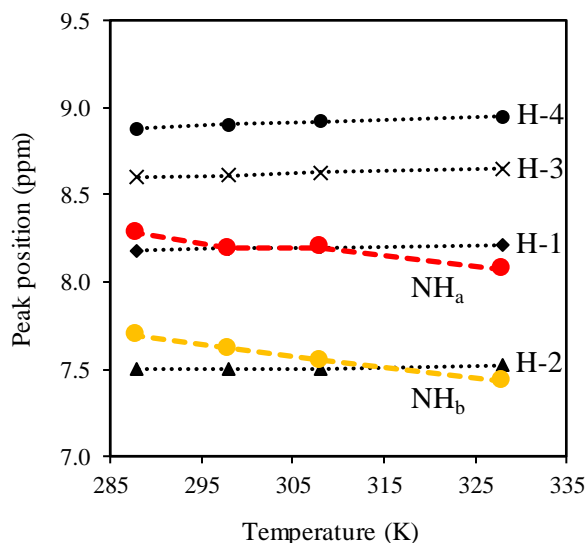
Figure 23. VT ^{1}H NMR spectra chemical shifts of [^{17}O]-nicotinamide. Red and yellow dots represent the two protons from NH$_2$ group while black circles, triangles, cross and diamonds represent the other four normal aromatic protons on nicotinamide. All the chemical shifts were referenced to H-2 on the aromatic ring as 7.5 ppm.

3.2.4   Conclusions

In this section, we report a QCT ^{17}O NMR study of [^{17}O]-nicotinamide. This is the first time that both P$_Q$ and P$_{SA}$ were determined simultaneously for an amide functional group in solution. At the ultraslow motion regime, because nicotinamide has a relatively large P$_{SA}$, the line width contribution from shielding anisotropy is now comparable with the second-order quadrupole term. This indicates there exists an optimal magnetic field to perform ^{17}O QCT NMR with best spectral resolution. This information can be used as a practical guide in future ^{17}O QCT studies of proteins. The experiments at low temperature also show the spectral resolution using QCT NMR can be even better than that obtained using conventional NMR method.

47

3.3 QCT ^{59}Co NMR of Vitamin B_{12} Derivatives

3.3.1 Introduction

Cobalt-59 has a nucleus of spin 7/2 with 100% natural abundance. ^{59}Co has a very large chemical shift range and has been one of the key nuclei that helped the development of the chemical shift theory.[54] The relaxation time of ^{59}Co is relative short; hence ^{59}Co is a relatively easily observed active nucleus for NMR studies of small molecules. However, ^{59}Co NMR spectra also suffer from quadrupole broadening like ^{17}O. Many solution-state ^{59}Co NMR studies have been reported in the past few decades. Kidd[55] discussed the various medium effects on ^{59}Co chemical shifts such as concentration, temperature, pressure, hydrogen-bonding and ion-pairing. Yamasaki[56] constructed and updated an extensive database on solution ^{59}Co chemical shifts. Chan et $al.$[57] also gave a thorough review on solid-state ^{59}Co NMR and advances in theoretical calculations of ^{59}Co NMR parameters. The ligand-field interpretation and parametrization of ^{59}Co chemical shifts were described in detail by Juranic.[58] Lately Wasylishen et $al.$ also reported the solid-state ^{13}C and ^{59}C NMR spectroscopy of ^{13}C-methylcobalt(III) complexes with amine ligands and showed the determination of the ^{59}Co nuclear quadrupolar parameters directly.[59]

Vitamin B_{12}, also called cobalamin, and other naturally occurring cobalamins are of great interest to scientists in the past years.[60,61] Despite a very low biological abundance, cobalt plays an important role in human's living system; it is an essential metal for people to maintain a normal physiology function. Vitamin B_{12} is a water-soluble vitamin containing cobalt that has a key role in the normal functioning of the brain and nervous system, and the formation of red blood cells. It is one of the eight B vitamins. It is involved in the metabolism of every cell of the human body, especially affecting DNA synthesis, fatty acid and amino acid metabolism. Humans cannot produce Vitamin B_{12} and have to absorb it from animal products such as various meat, fish, and

dairy products. Vitamin B_{12} is the most chemically complex molecule of all vitamins. The molecular structures of Vitamin B_{12} derivatives are shown in Fig. 24. They all contain a corrin ring and the central cobalt metal ion. Four of the six coordination sites are provided by the corrin ring, and a fifth by a dimethylbenzimidazole group. The sixth coordination site, the center of reactivity, is variable, being a cyano group (-CN), a methyl group (-CH$_3$), and a 5'-deoxyadenosyl group. They are called cyanocobalamin, methylcobalamin, coenzyme B_{12}, respectively.

R = 5'-deoxyadenosyl, Me, CN
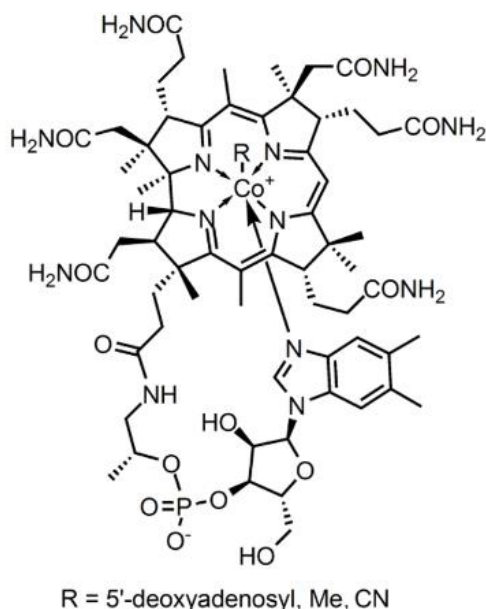
Figure 24. Molecular structures of the three vitamin B_{12} derivatives studied in the thesis.

Previous [59]Co NMR studies of Vitamin B_{12} compounds are mostly focused on solid-state NMR. Frydman *et al.*[62] showed that the quadrupolar coupling parameters of those vitamin B_{12} derivatives are quite sensitive to the type of ligands attached to the metal and the crystallization process. Extensive solid-state [59]Co, ^{13}C, ^{15}N and ^{31}P NMR studies have been reported for cyanocobalamin recrystallized from different solvents and under different conditions.[63] Two polymorphs are found which presumably correspond to the "wet" and "dry" cyanocobalamin structures of Hodgkin and co-workers.[64,65] Enlightened by previous studies of ^{17}O NMR using the

QCT method,[15] we apply the same QCT approach to study ^{59}Co NMR for Vitamin B_{12} derivatives in solution.

3.3.2 Experimental

All Vitamin B_{12} compounds were purchased from Sigma-Aldrich and used without further purification. All ^{59}Co NMR experiments were performed on Bruker Avance-400, -500, -600 MHz spectrometers. Normally solution samples were prepared in 5-mm NMR tubes and Bruker broadband solution probes were used to record the NMR spectra. All ^{59}Co chemical shifts are reported in ppm relative to the saturated $K_3Co(CN)_6$ solution in D_2O ($\delta(^{59}Co) = 0$ ppm) and by setting the ^{59}Co NMR signal of 0.5 M $Co(NH_3)_6Cl_3$ (aq) to $\delta(^{59}Co) = 8173$ ppm.[66] The effective 90 ^{o}C pulse is 3.5, 5.0 and 6.0 μs on Bruker Avance-400, -500 and -600 MHz spectrometers respectively.

3.3.3 Results and Discussion

Since the molecular weights of Vitamin B_{12} compounds are about 1000 Da, according to the estimation equation provided by Erickson[67] the volume should be around 1212 Å, which is almost ten times of those for glucose and nicotinamide, and therefore they tumble much more slowly in solution. For Vitamin B_{12} compounds in glycerol/water systems, the value of $\omega_0\tau_c$ is already in the slow motion range even at high temperatures. Fig. 25 shows the variable-temperature ^{59}Co NMR spectra of cyanocobalamin in various glycerol/water (w/w) systems. At the temperature range from 328 to 248 K, only the ^{59}Co CT signal can be observed. In addition, a common feature was observed in the QCT ^{59}Co NMR spectra. That is, the line width first decreases with the temperature until it reaches a minimum due to the dominance of the first-order quadrupole

interaction, then it increases with the further decrease of the temperature. In different solvent systems, each molecule has different correlation times due to the change of viscosity of solvent and thus various optimal temperatures are observed. This suggests that one may be able to select a solvent system so that the optimal resolution is observed at desired temperatures. The resolution seems to be consistent at different solvent systems. For example, the minimum line width was 7.73 kHz, 8.92 kHz, 7.14 kHz, 7.73 kHz and 7.73 kHz respectively at 9/1, 8/2, 7/3, 6/4 and 5/5 (glycerol/water, w/w) systems.
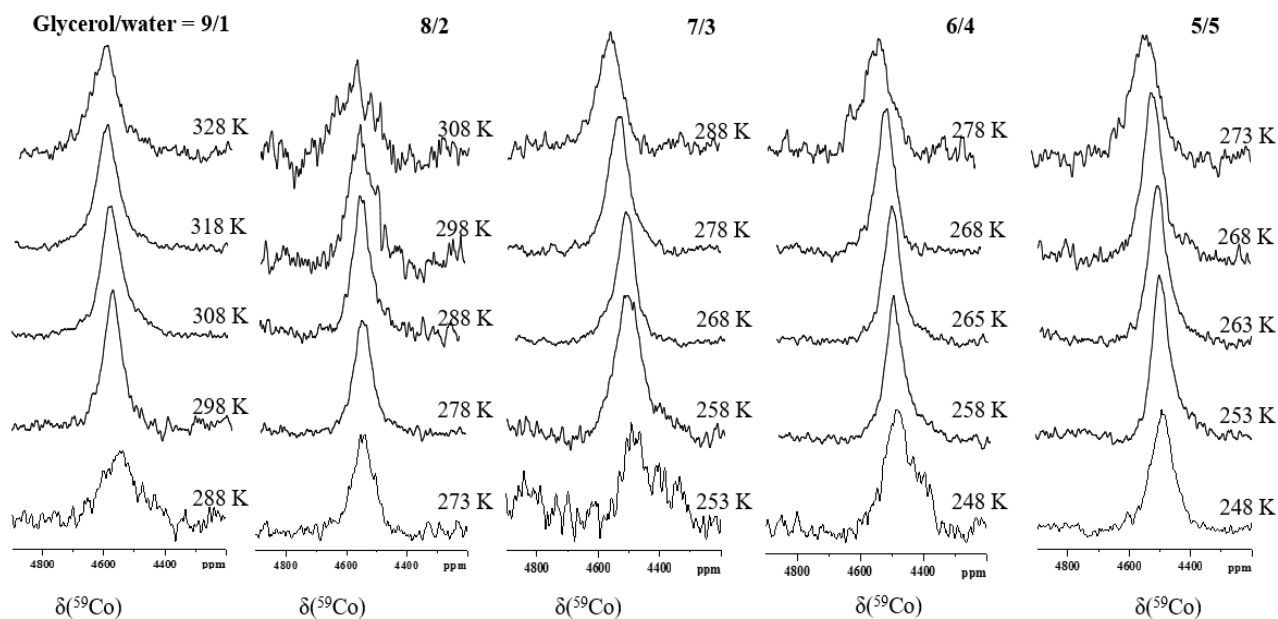
Figure 25. VT ^{59}Co NMR spectra of ~ 45 mg cyanocobalamin in 1 mL various glycerol/water (w/w) systems at 11.7 T.

Table 4 shows the measurement results of the cyanocobalamin line width at different solvent systems at various magnetic fields. The viscosities for different glycerol/water systems at various temperatures were calculated according to Cheng,[68] and the following equations were used:

Table 4. Solvent viscosity, molecular rotational correlation time, and ^{59}Co NMR line width for cyanocobalamin in different solvent systems (glycerol/water, w/w) at multiple magnetic fields.

9/1 at 14.1 T					9/1 at 11.7 T		
Temp (K)	η (mPa·s)	τ_c (ns)	$\omega_0\tau_c$	$\Delta\nu_{1/2}$ (kHz)	τ_c (ns)	$\omega_0\tau_c$	$\Delta\nu_{1/2}$ (kHz)
328	28.8	7.32	6.57	10.2	7.32	5.47	11.3
323	36.5	9.41	8.45	8.8	9.41	7.03	10.1
318	47.0	12.3	11.05	7.9	12.3	9.20	9.4
313	61.5	16.4	14.7	7.2	16.4	12.2	7.7
308	82.2	22.2	20.0	8.0	22.2	16.6	7.7
303	112	30.8	27.7	9.0	30.8	23.0	7.7
298	156	43.7	39.3	10.5	43.7	32.6	8.8
293	223	63.6	57.1	16.0	63.6	47.5	8.9
288	329	95.3				71.2	10.1
283	500	147				110	14.9

8/2 at 11.7 T					7/3 at 11.7 T				
Temp (K)	η (mPa·s)	τ_c (ns)	$\omega_0\tau_c$	$\Delta\nu_{1/2}$ (kHz)	Temp (K)	η (mPa·s)	τ_c (s)	$\omega_0\tau_c$	$\Delta\nu_{1/2}$ (kHz)
313	21.1	5.62	4.20	13.7	293	23.1	6.57	4.91	14.9
308	26.8	7.24	5.41	11.3	288	30.1	8.71	6.51	11.9
303	34.5	9.49	7.09	10.7	283	40.1	11.8	8.83	10.1
298	45.4	12.7	9.48	10.1	278	54.8	16.4	12.3	8.3
293	60.9	17.3	12.9	9.5	273	77.0	23.5	17.6	7.1
288	83.6	24.2	18.1	8.9	268	112	34.7	25.9	8.9
283	118	34.7	25.9	9.5	263	167	53.0	39.6	11.9
278	171	51.3	38.3	10.7	258	262	84.5	63.1	14.3
273	256	78.2	58.5	12.5					
313	21.1	5.62	4.20	13.7					

6/4 at 11.7 T					5/5 at 11.7 T				
Temp (K)	η (mPa·s)	τ_c (ns)	$\omega_0\tau_c$	$\Delta\nu_{1/2}$ (kHz)	Temp (K)	η (mPa·s)	τ_c (ns)	$\omega_0\tau_c$	$\Delta\nu_{1/2}$ (kHz)
278	22.8	6.83	5.10	16.1	273	14.6	4.45	3.33	13.7
273	30.4	9.28	6.94	9.5	268	19.2	5.96	4.45	9.7
268	41.7	13.0	9.69	8.3	263	25.9	8.20	6.12	8.3
263	58.9	18.7	14.0	7.7	258	36.0	11.6	8.69	7.7
258	86.3	27.9	20.8	8.3	253	52.0	17.1	12.8	7.7
253	131	43.4	32.4	10.7	248	78.2	26.3	19.6	10.1
248	211	70.8	52.9	12.5	243	124	42.5	31.7	16.1

* The uncertainty in $\Delta\nu_{1/2}$ is $\pm$ 0.1 kHz.

$$\mu = \mu_w^\alpha \mu_g^{1-\alpha} \tag{34}$$

$$\alpha = 1 - C_m + \frac{ab\, C_m(1-C_m)}{a\, C_m + b(1-C_m)} \tag{35}$$

$$\mu_w = 1.790\exp\left(\frac{(-1230-T)T}{36100+360T}\right) \tag{36}$$

$$\mu_g = 12100\exp\left(\frac{(-1233+T)T}{9900+70T}\right) \tag{37}$$

$$a = 0.705 - 0.0017T \tag{38}$$

$$b = (4.9 + 0.036T)a^{2.5} \tag{39}$$

where μ is the dynamic viscosity of the glycerol-water mixture, subscripts w and g denote water and glycerol respectively, and α is the weighting factor varying from 0 to 1. Cm is the glycerol concentration in mass, and a and b are the coefficients to determine the weighting factor α.
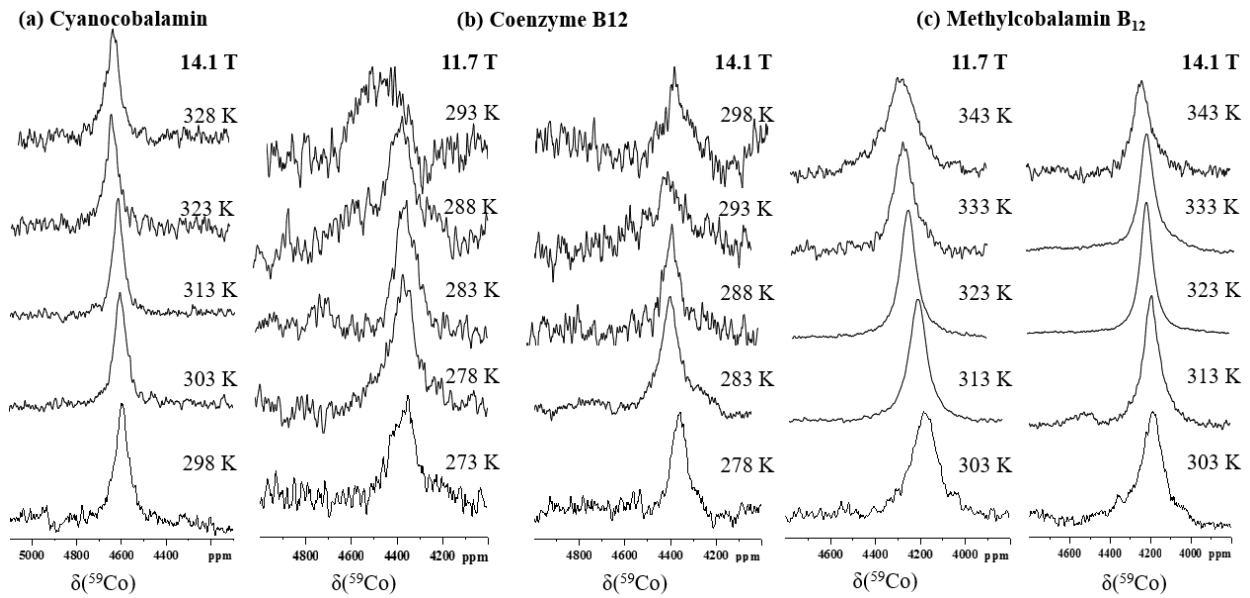
Figure 26. VT ^{59}Co NMR spectra of Vitamin B$_{12}$ derivatives in 1 mL different glycerol/water (w/w) systems. (a) 45 mg in 9/1 system (b) 18.5 mg Coenzyme in 7/3 system (c) 40 mg in 9/1 system.

Variable-temperature ^{59}Co NMR spectra of cyanocobalamin were also obtained at 14.1 T.

53

As can been seen from Fig. 26, the chemical shift was shifted to 4600 ppm at 14.1 T due to the dynamic frequency shift. Similar temperature dependences were observed at 14.1 T as that seen at 11. 7 T. The line width measurements of the other two Vitamin B_{12} derivatives were also conducted at 11.7 and 14.1 T. However, no significant improvement of the signal resolution was observed at higher frequencies. For example, the minimum ^{59}Co NMR line width of Coenzyme at 11.7 and 14.1 T are 10.5 and 11.0 kHz and those for methylcobalamin are 10.3 and 10.2 kHz respectively. These results suggests the comparable contribution from second-order quadrupole interaction and shielding anisotropy. Of course, more experiments at higher magnetic fields were needed to further confirm this deduction.
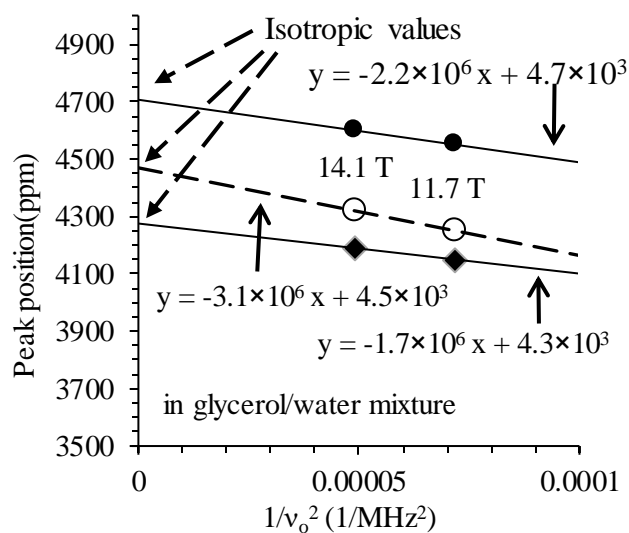
Figure 27. Observed ^{59}Co NMR peak positions for cyanocobalamin (black close circles), coenzyme B_{12} (black open circles) and methylcobalamin (black close diamonds).

The isotropic chemical shifts and P_Q values of Vitamin B_{12} derivatives were determined by plotting the chemical shifts of the Vitamin B_{12} compounds versus $1/v_0^2$, as shown in Fig. 27. The chemical shift values are 4700 ppm, 4500 ppm and 4300 ppm for cyanocobalamin, coenzyme B_{12} and methylcobalamin respectively, which are consistent with the literature values obtained in

aqueous solution.[62] The P_Q values were also determined in this way, which are 19.0 MHz, 22.6 MHz and 17.1 MHz for cyanocobalamin, coenzyme B_{12}, and methylcobalamin respectively. The P_Q values for cyanocobalamin and coenzyme B_{12} are in agreement with the literature values determined for the Vitamin B_{12} compounds after crystallization.[62] However, the P_Q value of methylcobalamin laid between the values that were measured without any purification and that slowly crystallized. Frydman *et al.*[62] suggested that the spectral variations may be due to the rearrangements of the axial ligands, or to conformational changes involving the cores of the corrinoid macrocycles. This is reasonable as the cobalt ligands may be undergoing substantially different conformational dynamics when various compounds are dissolved in solution of different viscosities. Of course, more measurements are needed at higher magnetic fields in order to get more accurate results.

Table 5. Solvent viscosity, molecular rotational correlation time, and ^{59}Co NMR line width for methylcobalamin B_{12} and coenzyme B_{12}.

Methylcobalamin B_{12}			11.7 T		14.1 T	
Temp (K)	η (mPa·s)	τ_c (ns)	$\omega_0\tau_c$	$\Delta\nu_{1/2}$ (kHz)	$\omega_0\tau_c$	$\Delta\nu_{1/2}$ (kHz)
343	15.4	9.14	6.83	19.7	8.21	12.5
338	18.8	11.3	8.43	14.6	10.1	12.2
333	23.1	14.1	10.5	11.5	12.7	11.0
328	28.8	17.8	13.3	10.3	16.0	10.2
323	36.5	23.0	17.2	10.7	20.6	10.2
318	47.0	30.0	22.4	11.0	27.0	10.7
313	61.5	40.0	29.9	13.5	35.9	13.0
308	82.2	54.2	40.5	14.8	48.7	13.2
303	112	75.2	56.2	19.1	67.5	16.1
298	156	107	79.7	24.4	95.8	19.0
Coenzyme B_{12}			11.7 T		14.1 T	
Temp (K)	η (mPa·s)	τ_c (ns)	$\omega_0\tau_c$	$\Delta\nu_{1/2}$ (kHz)	$\omega_0\tau_c$	$\Delta\nu_{1/2}$ (kHz)
293	23.1	11.8	8.81	17.8	10.6	14.6
288	30.1	15.6	11.7	14.0	14.1	11.0
283	40.1	21.2	15.9	10.5	19.1	11.7
278	54.8	29.5	22.0	11.3	26.5	11.9
273	77.0	42.2	31.5	13.1		
* The uncertainty in $\Delta\nu_{1/2}$ is ± 0.1 kHz.						

Table 5 show the raw data line width of coenzyme B_{12} and methylcobalamin B_{12} at various

temperatures at multiple magnetic fields. The viscosities were calculated based on Cheng,[68] and τ_c were calculated based on the SED model using eq. (9). The correlation time covers the slow motion range ($\omega_0\tau_c = 6.83$ to $\omega_0\tau_c = 95.8$).

To further analyze line width data for these B_{12} compounds, eq. (23) was used for fitting. Fig. 28 shows the experimental line width of cyanocobalamin, coenzyme B_{12} and methylcobalamin B_{12} at multiple magnetic fields and the theoretical curves were calculated with eq. (23). As shown in Fig. 28 (a) and (b), a simultaneous fit of cyanocobalamin line width at different solvent systems at two magnetic fields produced the following parameters: $V_h = 1436$ Å^3, $P_Q = 27$ MHz, $P_{SA} = 3300$ ppm. Fig. 28 (a) shows one distinct advantage of doing ^{59}Co QCT NMR of Vitamin B_{12} and its analogs, which is the tunable τ_c resulting from the change of solvent viscosity. In this way, the optimal temperature can be adjusted. By changing the viscosity of solvent, the minimum line width was achieved at different temperatures. For example, for 9/1 (glycerol/water, w/w) system, the optimal temperature was 308 K; while for 5/5 (glycerol/water, w/w) system, the optimal temperature was significantly shifted to 253 K. This indicates great used of QCT NMR as researcher can now choose the desired optimal temperature. For coenzyme B_{12}, as shown in Fig. 28 (c), the parameters are: $V_h = 2064$ Å^3, $P_Q = 23$ MHz, $P_{SA} = 3300$ ppm. By fitting Fig. 28. (d), the following parameters were yielded for methylcobalamin B_{12}: $V_h = 2064$ Å^3, $P_Q = 20.5$ MHz and $P_{SA} = 3300$ ppm. The molecular volumes of cyanocobalamin and its analogs are reasonable and are consistent with the literature value.[67] This indicates that for biological macromolecules, whose molecular sizes are much larger than small organic molecules such as glucose and nicotinamide, the effective volume is not that sensitive to solvent molecules even in the presence of hydrogen bond, thus SED model can be applied successfully. P_Q is also consistent with those obtained using solid-state ^{59}Co NMR.[62] However, P_{SA} values of Vitamin B_{12} compounds are

56

considerably different from the parameters obtained by solid-state ^{59}Co NMR.[62] This discrepancy may due to the different detecting conditions of the molecules. As for QCT NMR technique, the molecules are surrounded by solvent molecules while in solid-state NMR, the target molecules are in the form of solid powder.
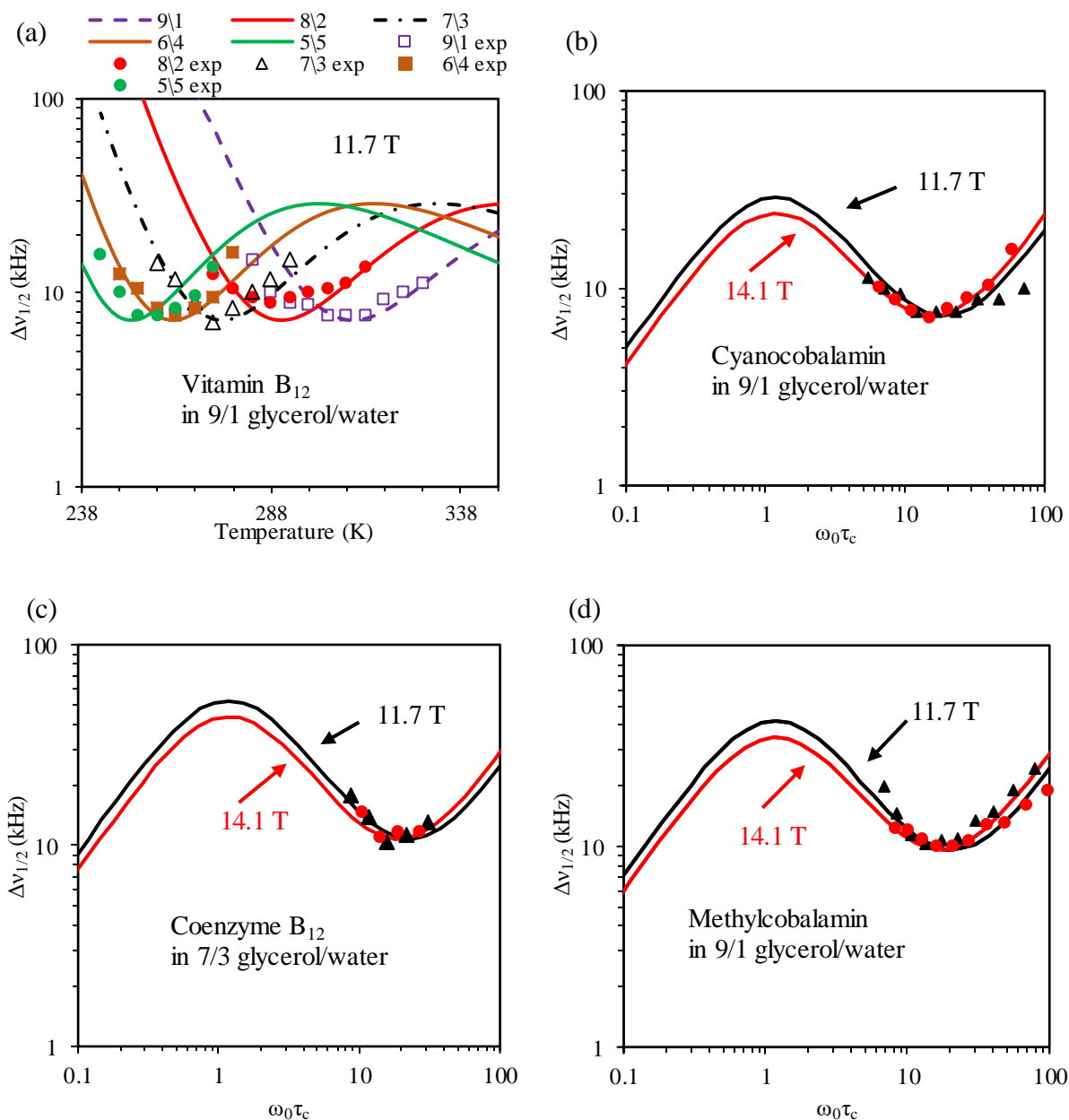
Figure 28. Experimental line width of Vitamin B$_{12}$ derivatives in various glycerol/water (w/w) systems. All the theoretical curves were calculated based on eq. (23) with the parameters given in the text.

3.3.4 Conclusions

In this section, we have report a ^{59}Co QCT NMR study of three Vitamin B_{12} derivatives. This is the first ^{59}Co QCT NMR study and this series of experiments also shows that for molecules with larger size, the QCT NMR is still applicable. We show that P_Q and P_{SA} were simultaneously determined. By using solvents of different viscosities, the optimal temperature of the spectra can be changed as well. This indicates QCT NMR may become a common technique for biological large molecules in the future. These experiments suggest the QCT NMR can also be further generalized to other quadrupolar nuclei such as ^{23}Na (I = 3/2) and ^{27}Al (I = 5/2).

Chapter 4   Conclusions and Future Work

We have reported extensive ^{17}O and ^{59}Co QCT NMR results for three classes of biologically important molecules: glucose, nicotinamide, and Vitamin B_{12} derivatives. We demonstrated great potential of QCT NMR as a standard technique to study both small organic molecules and complex biological macromolecules in solution. A series of NMR parameters such as P_Q, P_{SA} and hydrodynamic volumes were obtained for glucose, nicotinamide and Vitamin B_{12} derivatives. For glucose, under slow motion, the first-order quadrupole interaction dominates, thus there exists a minimum value until the molecule reaches the ultraslow motion when the second-order quadrupole interaction becomes the dominating NMR relaxation mechanism. This is the first experimental confirmation of this new relaxation mechanism at the ultraslow motion regime.[69] For nicotinamide, however, at the ultraslow motion regime, the second-order quadrupole interaction is comparable with the shielding anisotropy component because of its larger P_{SA} value. The parameters obtained for glucose and nicotinamide provide information on hydroxyl and amide groups, which may be important to understand the behavior of amino acids and proteins in the future. For Vitamin B_{12} derivatives, we reported the first ^{59}Co QCT NMR study. Our results suggest that more research need to be conducted to generalize the QCT NMR technique.

In the future, a larger range of molecules of different sizes and particular functional groups should also be investigated using this method to provide more information on biological macromolecules such as peptides, proteins, DNA and RNA. Different quadrupolar nuclei such as ^{23}Na (I = 3/2), ^{27}Al (I = 5/2), etc., could also be further studied using QCT NMR. Since most of the biological molecules are usually in the slow motion ranges, using QCT NMR would be of particular interest due to the properties of relaxation mechanism. In addition, since the

measurements are conducted in solution, a lot of information can be yielded during the reaction process, such as catching kinetically competent intermediates or studying chemical reaction mechanism. With that, more insight would be yielded in terms of biological mechanism and structure determination. The main challenge in future for ^{17}O QCT NMR would be the isotopic labelling of large biological molecules.[70] It may also be possible to extend the QCT approach to paramagnetic systems.[71]

References

(1)   Ogg, R. A.; Ray, J. D. *J. Chem. Phys.* **1957**, *26*, 1339-1340.
(2)   Werbelow, L. G. *J. Chem. Phys.* **1996**, *104*, 3457-3462.
(3)   Laws, D. D.; Bitter, H. L.; Jerschow, A. *Angew. Chem. Int. Ed. Engl.* **2002**, *41*, 3096-3129.
(4)   Drechsler, A.; Separovic, F. *IUBMB. Life.* **2003**, *55*, 515-523.
(5)   Wu, G. *Biochem. Cell Biol.* **1998**, *76*, 429-442.
(6)   Redfield, A. G. *Adv. Magn. Reson.* **1966**, *1*, 1-32.
(7)   Baram, A.; Luz, Z.; Alexander, S. *J. Chem. Phys.* **1973**, *58*, 4558-4564.
(8)   Butler, A.; Eckert, H. *J. Am. Chem. Soc.* **1989**, *111*, 2802-2809.
(9)   Lee, H. C.; Oldfield, E. *J. Am. Chem. Soc.* **1989**, *111*, 1584-1590.
(10)   Aramini, J. M.; Germann, M. W.; Vogel, H. J. *J. Am. Chem. Soc.* **1993**, *115*, 9750-9753.
(11)   Germann, M. W.; Aramini, J. M.; Vogel, H. J. *J. Am. Chem. Soc.* **1994**, *116*, 6971-6972.
(12)   Aramini, J. M.; McIntyre, D. D.; Vogel, H. J. *J. Am. Chem. Soc.* **1994**, *116*, 11506-11511.
(13)   Aramini, J. M.; Vogel, H. J. *J. Am. Chem. Soc.* **1994**, *116*, 1988-1993.
(14)   Aramini, M. J.; Vogel, J. H. *Biochem. Cell Biol.* **1998**, *76*, 210-222.
(15)   Zhu, J.; Wu, G. *J. Am. Chem. Soc.* **2011**, *133*, 920-932.
(16)   Zhu, J.; Kuan, I. C. M.; Wu, G. *J. Am. Chem. Soc.* **2009**, *131*, 14206-14207.
(17)   Young, R. P.; Caulkins, B. G.; Borchardt, D.; Bulloch, D. N.; Larive, C. K.; Dunn, M. F.; Mueller, L. J. *Angew. Chem. Int. Ed. Engl.* **2016**, *55*, 1350-1354.
(18)   Zhu, J.; Ye, E.; Terskikh, V.; Wu, G. *J. Phys. Chem. Lett.* **2011**, *2*, 1020-1023.
(19)   Westlund, P.; Wennerstrom, H. *J. Magn. Reson.* **1982**, *50*, 451-466.
(20)   Wu, G. *J. Magn. Reson.* **2016**, *269*, 176-178.
(21)   Roy, M.; Doraiswamy, S. *J. Chem. Phys.* **1993**, *98*, 3213-3223.
(22)   Abragam, A. *The Principles of Nuclear Magnetism*; Oxford University Press: Lodon, 1961.
(23)   Hubbard, P. S. *J. Chem. Phys.* **1970**, *53*, 985-987.
(24)   Bull, T. E. *J. Magn. Reson.* **1972**, *8*, 344-353.
(25)   Bull, T. E.; Forsén, S.; Turner, D. L. *J. Chem. Phys.* **1979**, *70*, 3106-3111.
(26)   Spiess, H. W. In *NMR Principles and Progress*; Diehl, P., Fluck, E., Kosfeild, R., Eds.; Springer-Verlag: Berlin: 1978; Vol. 15, p 55-214.
(27)   Werbelow, L. *J. Phys. Chem.* **1981**, *85*, 3887-3891.
(28)   Zhu, J.; Kurahashi, T.; Fujii, H.; Wu, G. *Chem. Sci.* **2012**, *3*, 391-397.
(29)   Yamada, K.; Dong, S.; G., W. *J. Am. Chem. Soc.* **2000**, *122*, 11602-11609.
(30)   Chekmenev, Y. E.; Waddell, W. K.; Hu, J.; Gan, Z.; Wittebort, J. R.; T., C. A. *J. Am. Chem. Soc.* **2006**, *128*, 9849-9855.
(31)   Sefzik, T. H.; Houseknecht, J. B.; Clark, T. M.; Prasad, S.; Lowary, T. L.; Gan, Z.; Grandinetti, P. J. *Chem. Phys. Lett.* **2007**, *434*, 312-315.
(32)   Wu, G.; Zhu, J.; Mo, X.; Wang, R.; Terskikh, V. *J. Am. Chem. Soc.* **2010**, *132*, 5143-5155.
(33)   Ochi, K.; Okui, K. *Chem. Pharm. Bull.* **1974**, *22*, 2223-2230.
(34)   Dirken, P. J.; Smith, M. E.; Whitfield, H. J. *J. Phys. Chem.* **1995**, *99*, 395-401.

(35)   Bull, L. M.; Cheetham, A. K.; Anupold, T.; Reinhold, A.; Samoson, A.; Sauer, J.; Bussemer, B.; Lee, Y.; Gann, S.; Shore, J.; Pines, A.; Dupree, R. *J. Am. Chem. Soc.* **1998**, *120*, 3510-3511.

(36)   Schramm, S.; Oldfield, E. *J. Am. Chem. Soc.* **1984**, *106*, 2502-2506.

(37)   Yamauchi, K.; Kuroki, S.; Ando, I.; Ozaki, T.; Shoji, A. *Chem. Phys. Lett.* **1999**, *302*, 331-336.

(38)   Wu, G. *Prog. Nucl. Magn. Reson. Spectrosc.* **2008**, *52*, 118-169.

(39)   Wu, G. *Solid. State. Nucl. Magn. Reson.* **2016**, *73*, 1-14.

(40)   Zhu, J.; Geris, J. A.; Wu, G. *Phys. Chem. Chem. Phys.* **2009**, *11*, 6861-7088.

(41)   Mackie, W.; Perlin, A. S. *Can. J. Chem* **1965**, *43*, 2921-2924.

(42)   Yamauchi, N.; K., K. *J. Org. Chem.* **1995**, *60*, 5614-5619.

(43)   Chan, J.; Tang, A.; Bennet, A. J. *J. Am. Chem. Soc.* **2012**, *134*, 1212-1220.

(44)   Gerothanassia, I. P.; Lauterwein, J.; Sheppard, N. *J. Magn. Reson.* **1982**, *48*, 431-446.

(45)   Schulte, J.; Lauterwein, J. *J. Magn. Reson.* **1993**, *101*, 95-97.

(46)   Werbelow, L. G. *J. Chem. Phys.* **1979**, *70*, 5381-5383.

(47)   Crittenden, J. C.; Trussell, R. R.; Hand, D. W.; Howe, K. J.; Tchobanoglous, G. In *MWH's Water Tretment: Principles and Design*; 3rd ed.; Wiley: 2012.

(48)   Trejo González, J. A.; Longinotti, M. P.; Corti, H. R. *J. Chem. Eng. Data.* **2011**, *56*, 1397-1406.

(49)   Banipal, P. K.; Banipal, T. S.; Larkb, B. S.; Ahluwalia, J. C. *J. Chem. Soc. Faraday Trans.* **1997**, *93*, 81-87.

(50)   Khodaeiani, E.; Fouladi, F. R.; Amirnia, M.; Saeidi, M.; Karimi, R. E. *Int. J. Derm.* **2013**, *52*, 999-1004.

(51)   Surjana, D.; Halliday, G. M.; Martin, A. J.; Moloney, F. J.; Damian, D. L. *J. Invest. Dermatol.* **2012**, *132*, 1497-1500.

(52)   Kolodziejska-Huben, M.; Kaminski, Z.; Paneth, P. *J. Label. Compd. Radiopharm.* **2002**, *45*, 1005-1010.

(53)   Wright, W. B.; King, G. S. D. *Acta. Cryst.* **1954**, *7*, 283-288.

(54)   Proctor, W. G.; Yu, F. C. *Phys. Rev.* **1951**, *81*, 20-30.

(55)   Kidd, R. G.; Goodfellow, R. J. In *NMR and the Periodic Table*; Harris, R. K., Mann, B. E., Eds.; Academic Press London: 1978.

(56)   Yamasaki, A. *J. Coord. Chem.* **1991**, *24*, 211-260.

(57)   Chan, J. C. C.; Au-Yeung, S. C. F. *Annu. Rep. NMR Spectrosc.* **2000**, *41*, 1-54.

(58)   Juranic, N. *Coord. Chem. Rev.* **1989**, *96*, 253-290.

(59)   Ooms, K. J.; Bernard, G. M.; Kadziola, A.; Kofod, P.; Wasylishen, R. E. *Phys. Chem. Chem. Phys.* **2009**, *11*, 2690-2699.

(60)   Scot, A. I. *Pure and Applied Chem.* **1996**, *68*, 2057-2063.

(61)   Battersby, A. R.; Leeper, F. J. *Top. Curr. Chem.* **1998**, *195*, 143-193.

(62)   Medek, A.; Frydman, V.; Frydman, L. *Proc. Natl. Acad. Sci.* **1997**, *94*, 14237-14242.

(63)   Medek, A.; Frydman, L. *J. Am. Chem. Soc.* **2000**, *122*, 684-691.

(64)   Brink-Shoemaker, D.; Cruikshank, D. W. J.; Hodgkin, D. C.; Kamper, D. J.; Pilling, D. *Proc. R. Soc. A* **1964**, *278*, 1-30.

(65)   Hodgkin, D. C.; Lindsey, J.; Sparks, R. A.; Trueblood, K. N.; White, J. G. *Proc. R. Soc. A* **1962**, *266*, 494-517.

(66)   Bendall, M. R.; Doddrell, D. M. *J. Magn. Reson.* **1979**, *33*, 659-663.

(67)   Erickson, H. P. *Biol. Proced. Online.* **2009**, *11*, 32-51.

(68)   Cheng, N. *Ind. Eng. Chem. Res.* **2008**, 3285-3288.

(69)   Shen, J.; Terskikh, V.; Wu, G. *J. Phys. Chem. Lett.* **2016**, 3412-3418.

(70)   Zhu, J.; Ye, E.; Terskikh, V.; Wu, G. *Angew. Chem. Int. Ed. Engl.* **2010**, *49*, 8399-8402.

(71)   Kong, X.; Terskikh, V.; Khade, R.; Yang, L.; Rorick, A.; Zhang, Y.; He, P.; Huang, Y.; Wu, G. *Angew. Chem. Int. Ed. Engl.* **2015**, 4753-4757.

Appendix I Supplementary NMR data
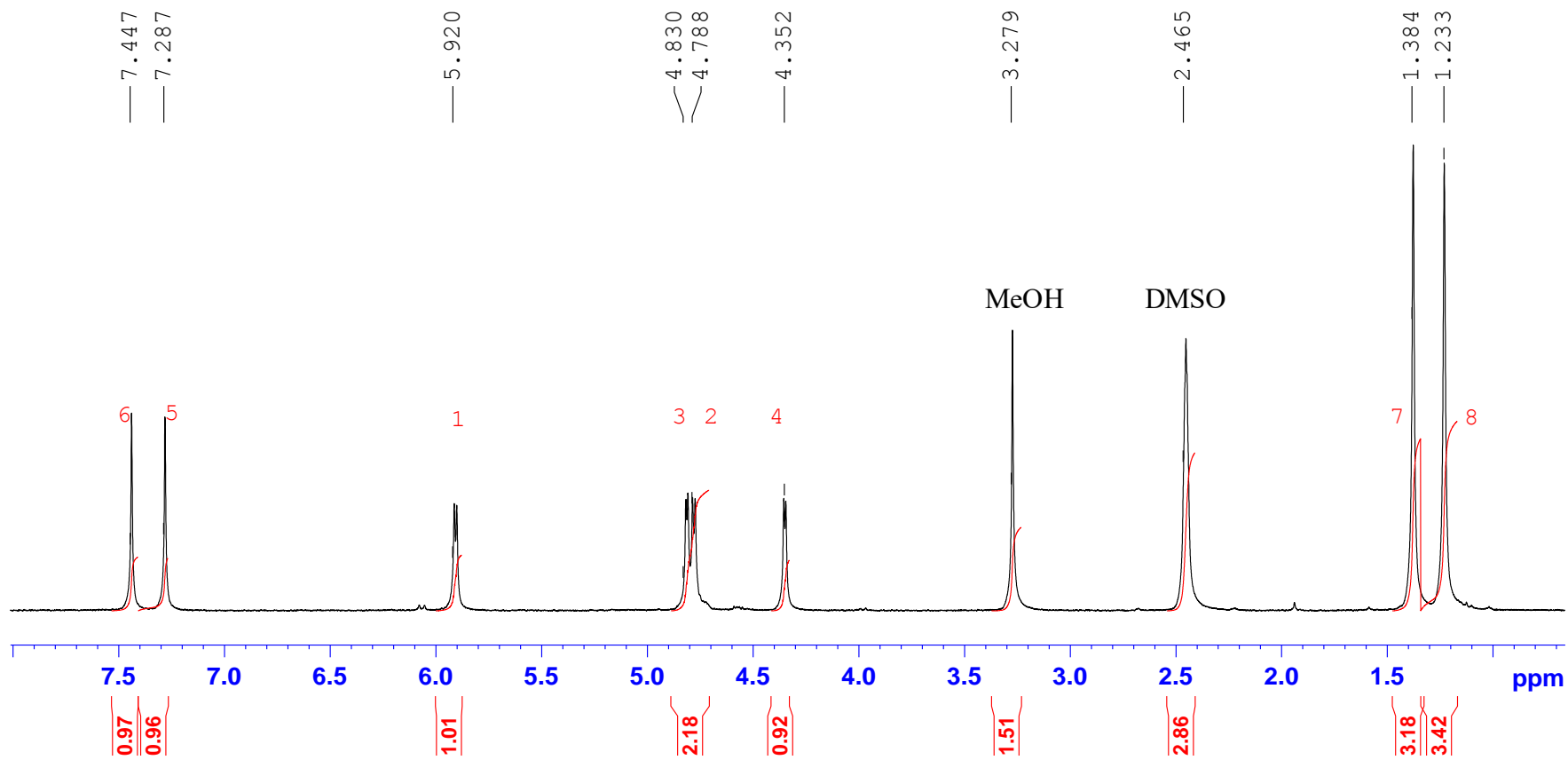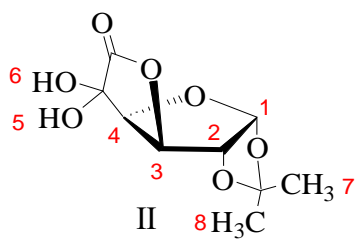
Figure A-1. ^{1}H NMR spectrum of 1, 2-O-isopropylidene-D-xylo-hexofuranurono-6, 3-lactone-5-ulose hydrate in DMSO-d$_6$ at 7.1 T.

A-1
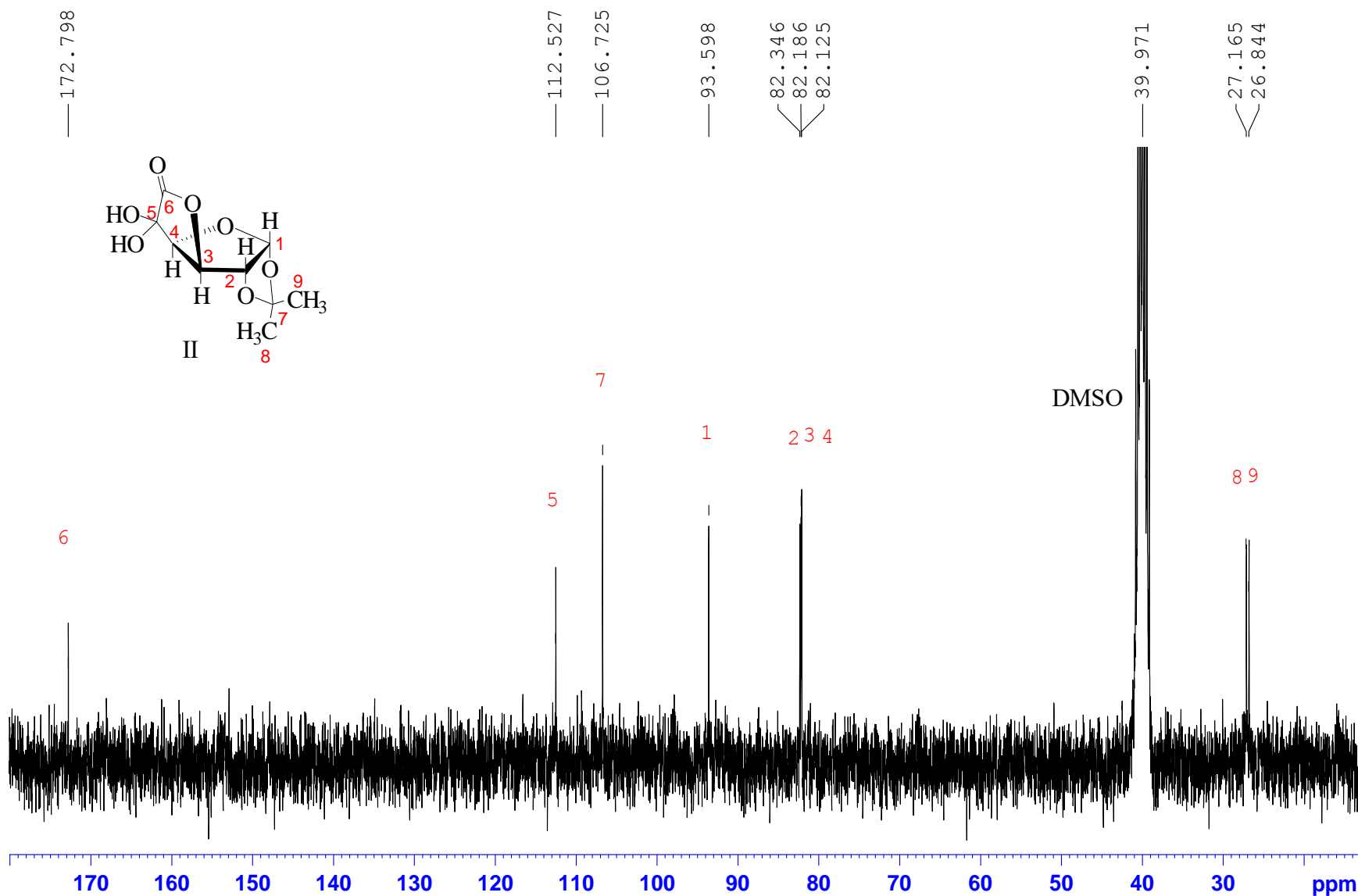
Figure A-2. ^{13}C NMR spectrum of 1, 2-O-isopropylidene-D-xylo-hexofuranurono-6, 3-lactone-5-ulose hydrate in DMSO-d_6 at 7.1 T.

A-2
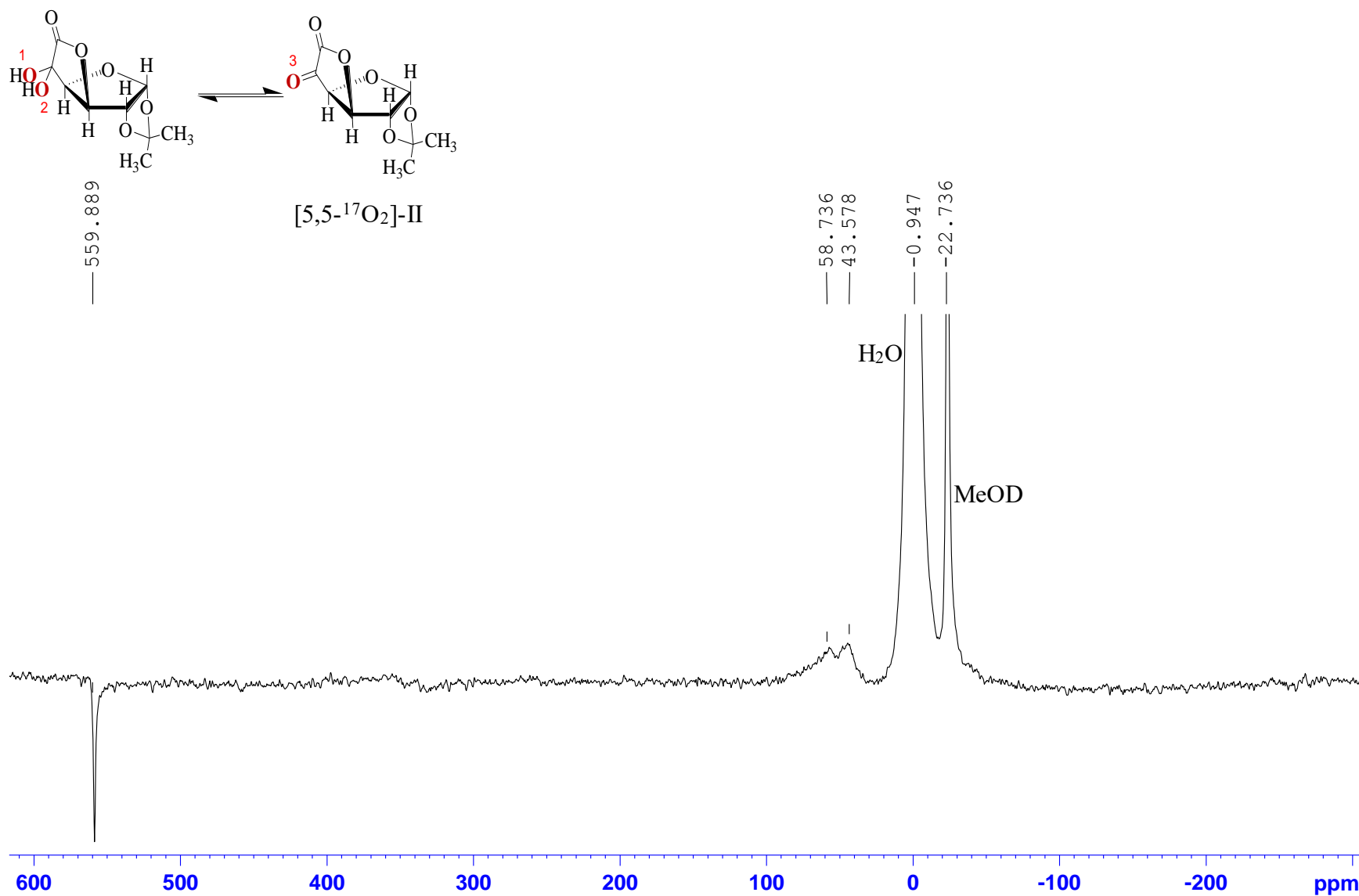
Figure A-3. ^{17}O NMR spectrum of [5,5-$^{17}O_2$]-1, 2-O-isopropylidene-D-xylo-hexofuranurono-6, 3-lactone-5-ulose hydrate in methanol-d$_4$ at 11.7 T.

A-3
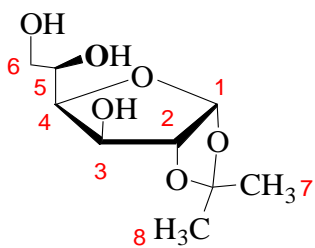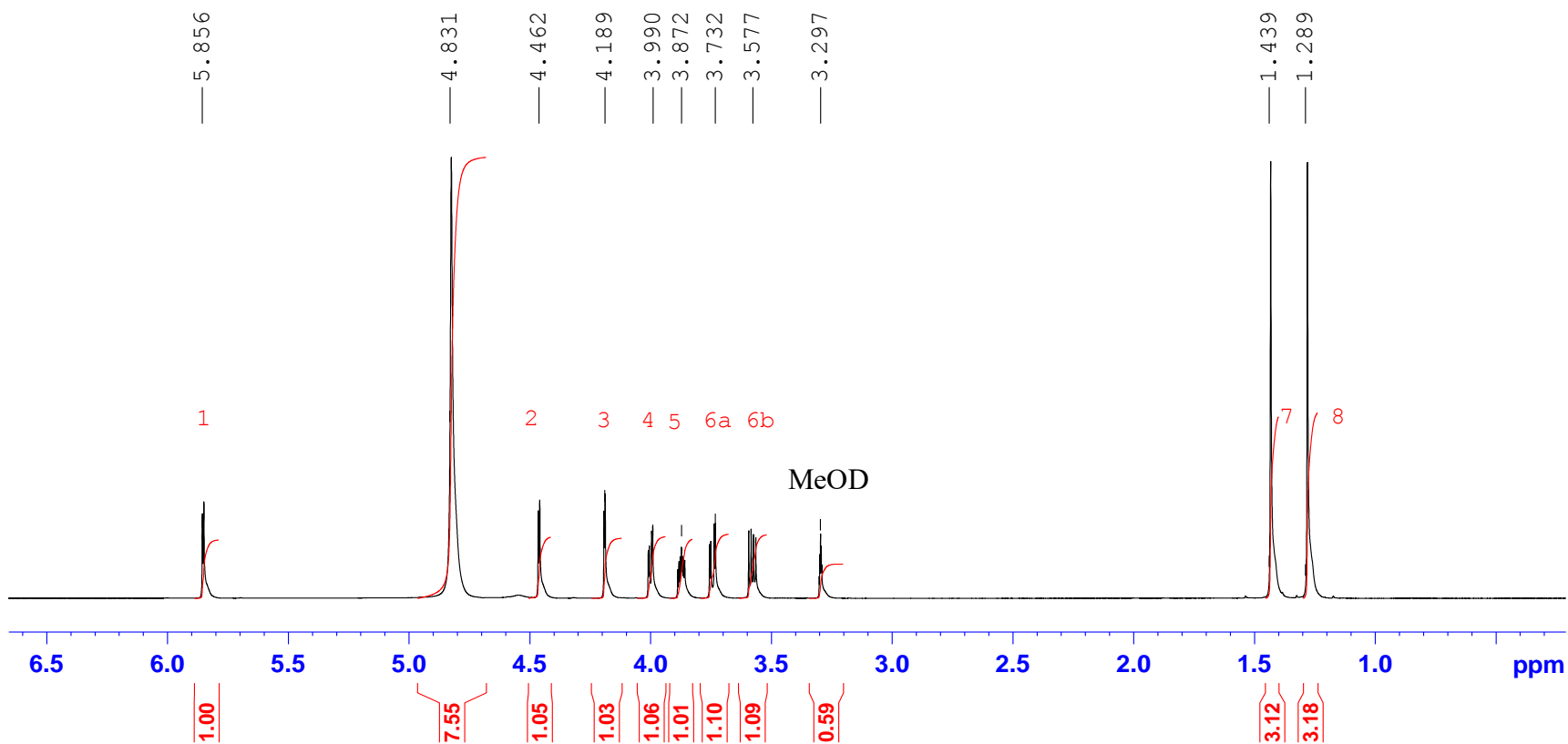
Figure A-4. ^{1}H NMR of 1, 2-O-isopropylidene-α-D-[5-^{17}O]-glucofuranose in methanol-d$_4$ at 14.1 T.
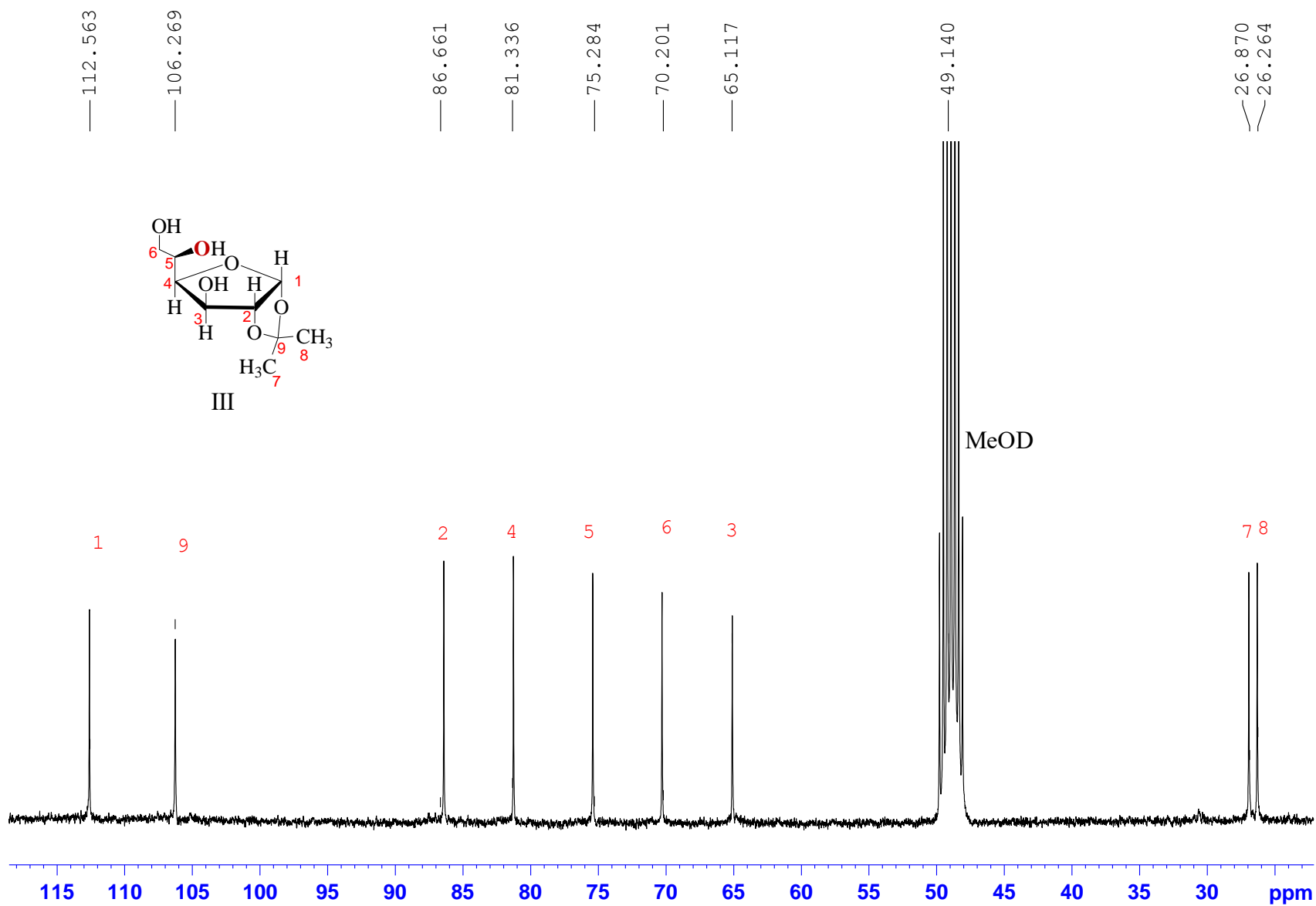
Figure A-5. ^{13}C NMR of 1, 2-O-isopropylidene-α-D-[5-^{17}O]-glucofuranose in methanol-d_4 at 7.1 T.

A-5
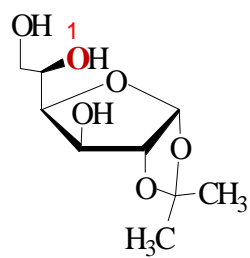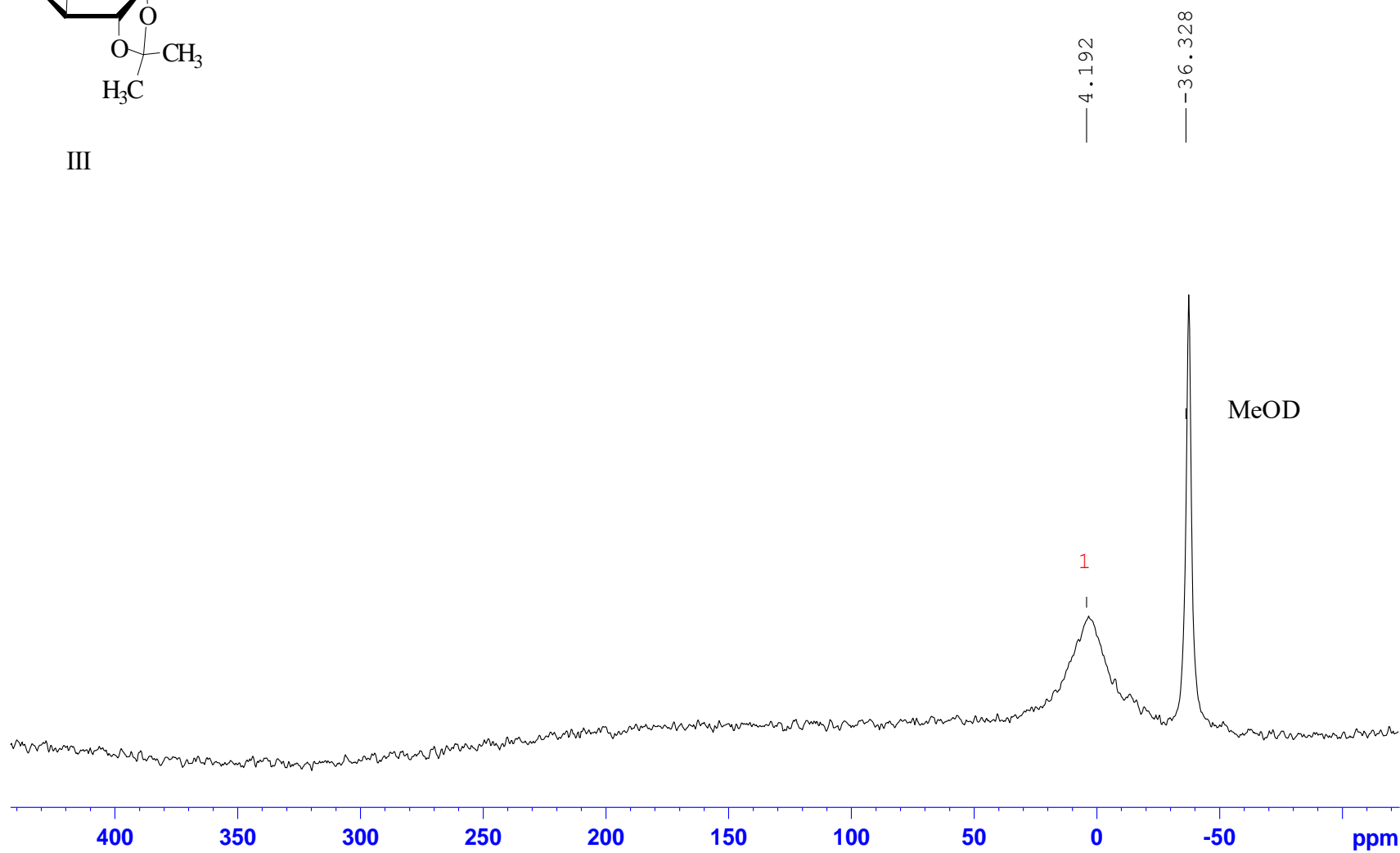
Figure A-6. ^{17}O NMR spectrum of 1, 2-O-isopropylidene-α-D-[5-^{17}O]-glucofuranose in methanol-d4 at 14.1 T.
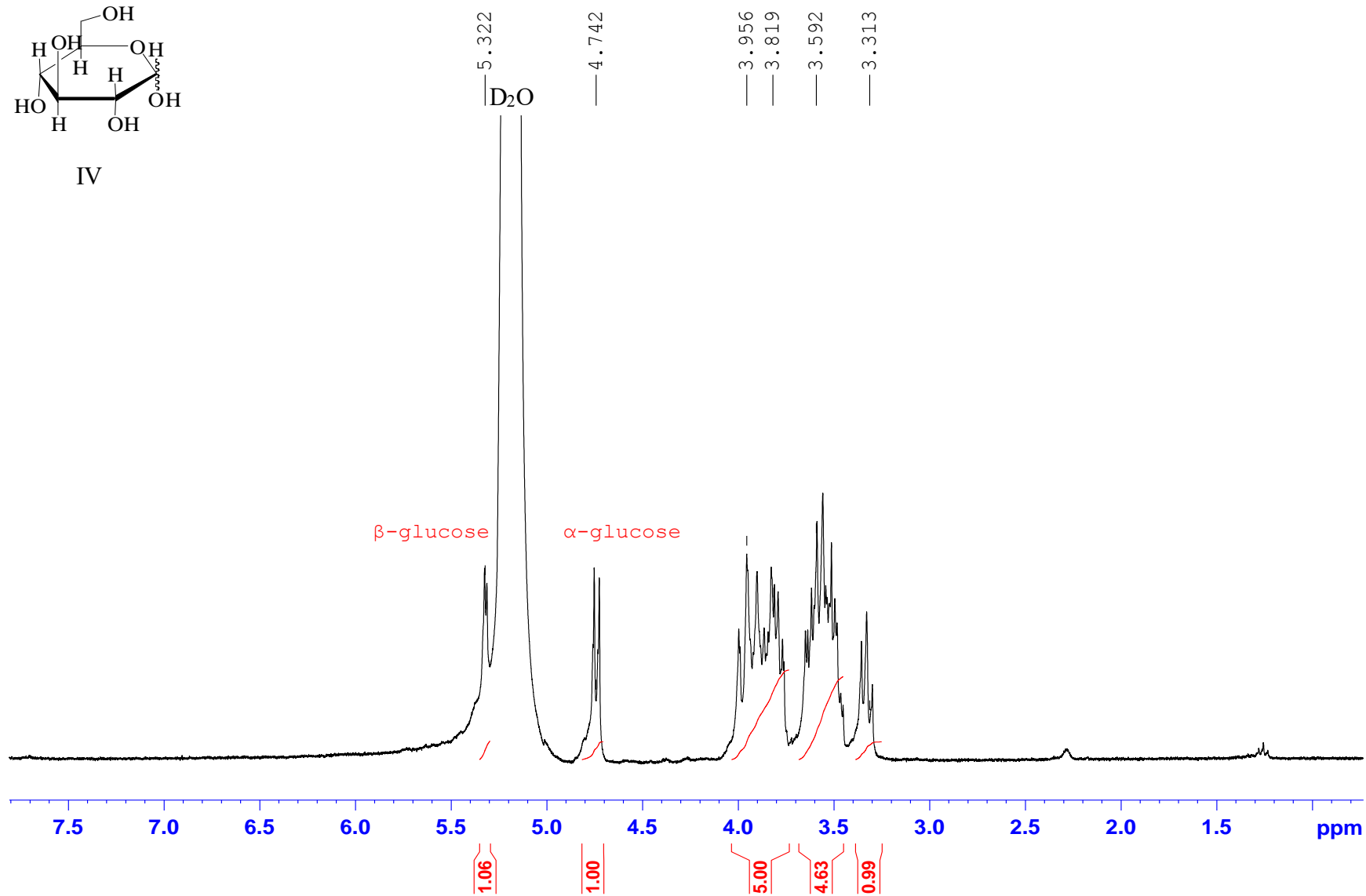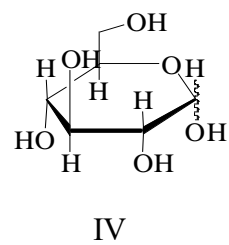
Figure A-7. ^{1}H NMR of D-[5-^{17}O]-glucose in D$_2$O at 7.1 T.

A-7
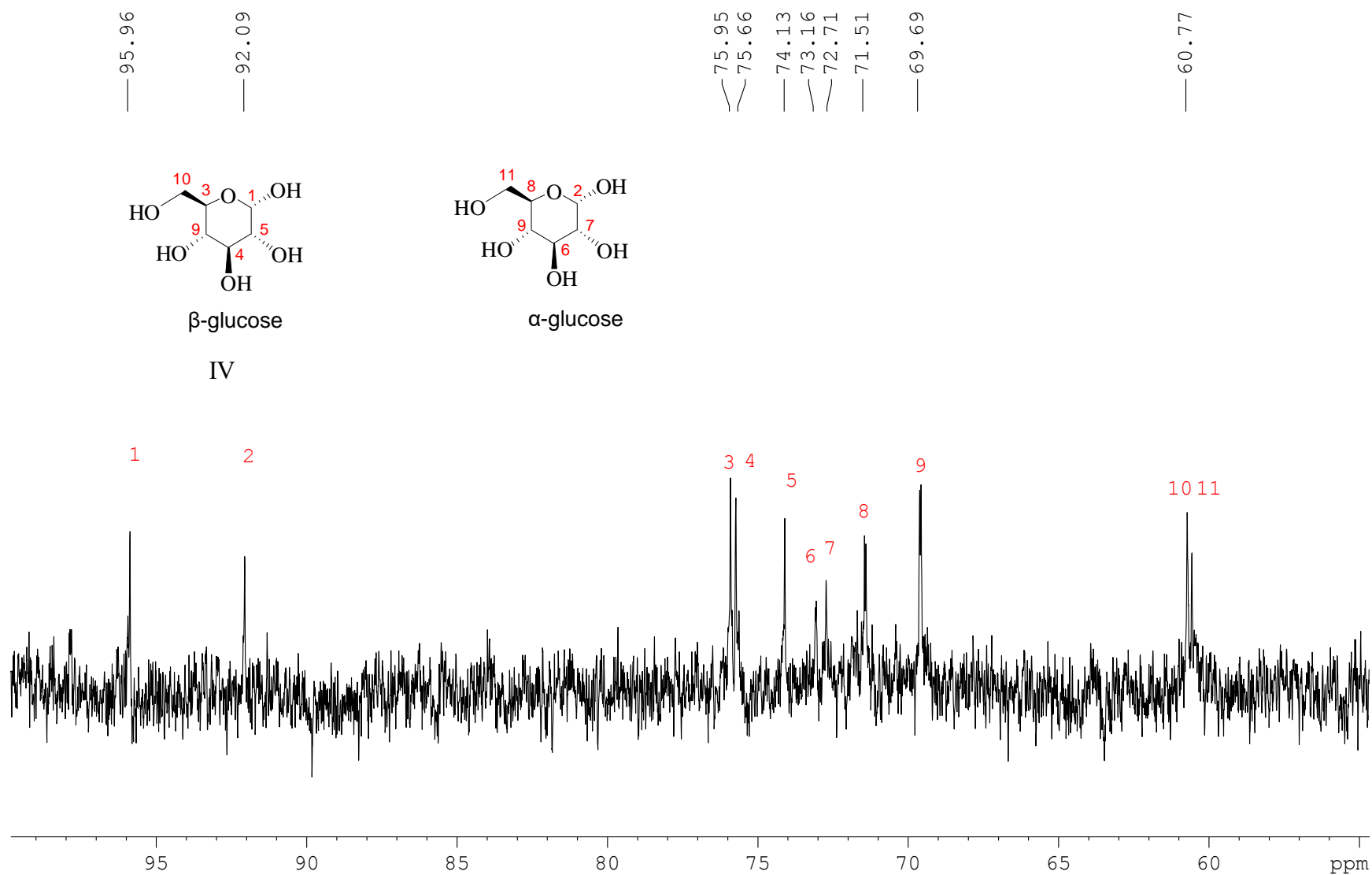
Figure A-8. ^{13}C NMR of D-[5-^{17}O]-glucose in D_2O at 7.1 T.
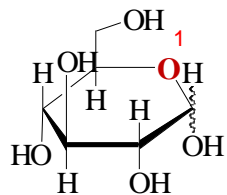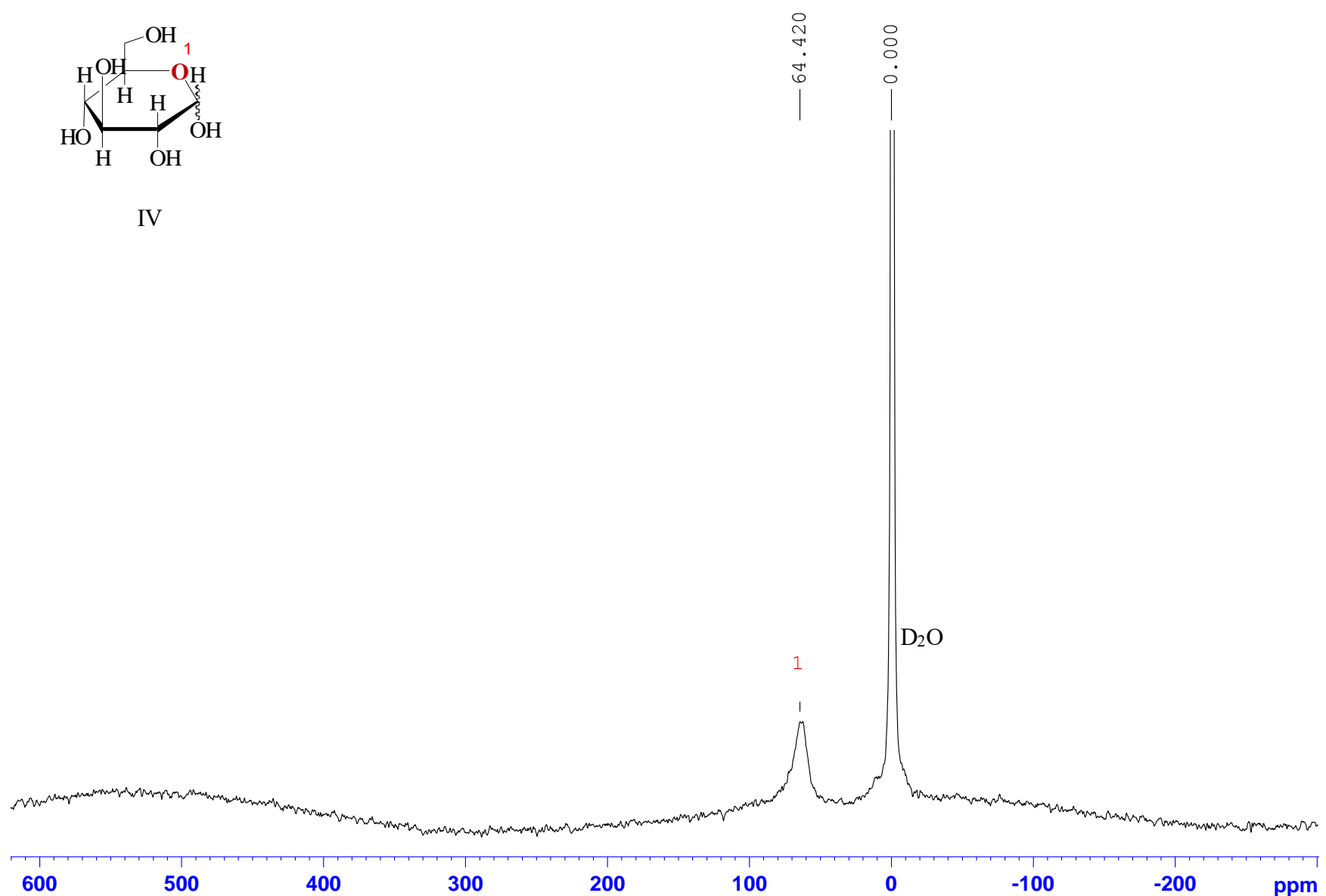
Figure A-9. ^{17}O NMR spectrum of D-[5-^{17}O]-glucose in D_2O at 7.1 T, 355 K.

A-9
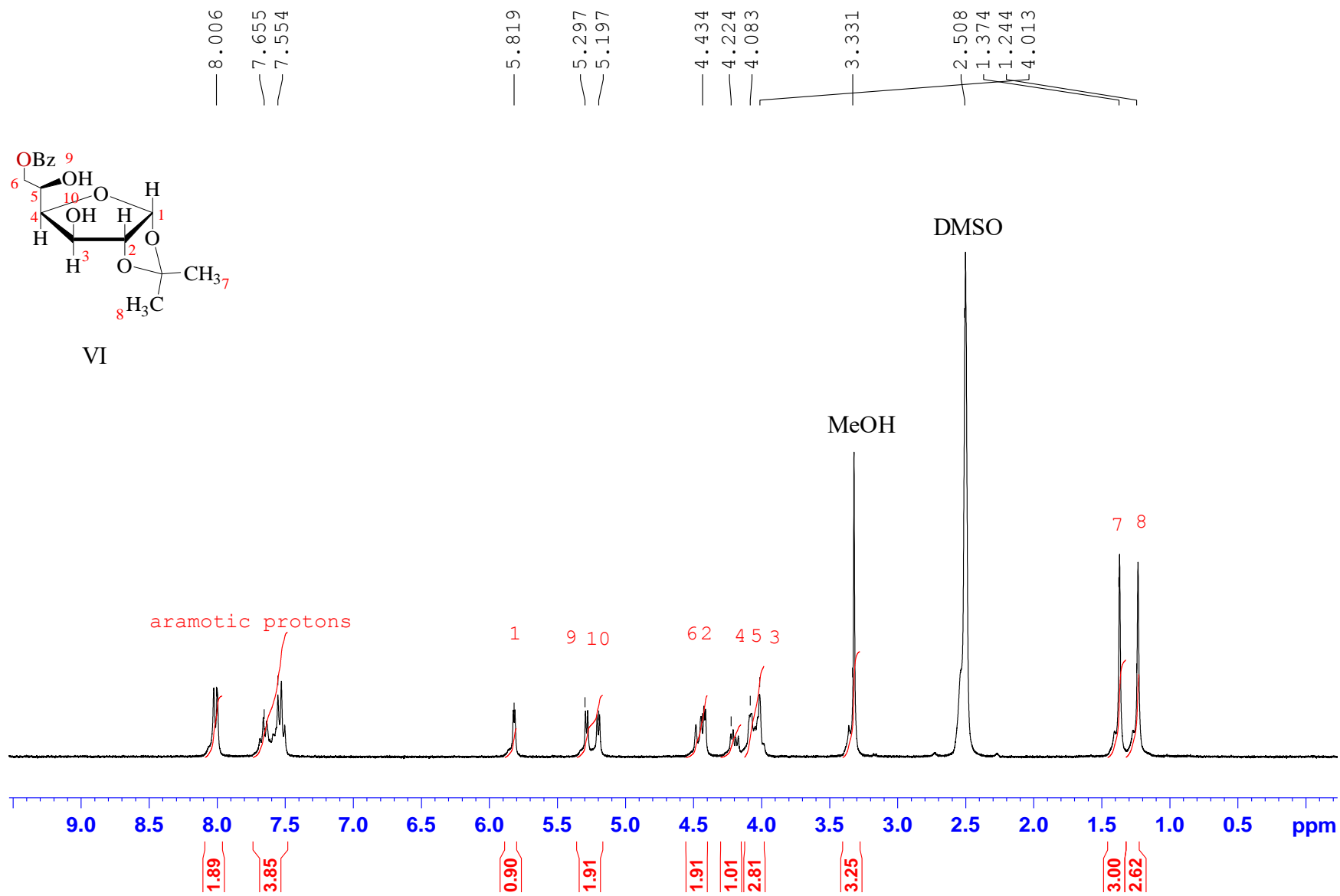
Figure A-10. ^{1}H NMR of [6-^{17}O]-Benzoyl-1, 2-O-isopropylidene-α-D-glucofuranose in DMSO-d$_6$ at 7.1 T.
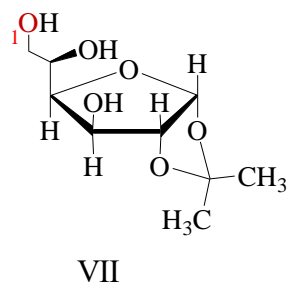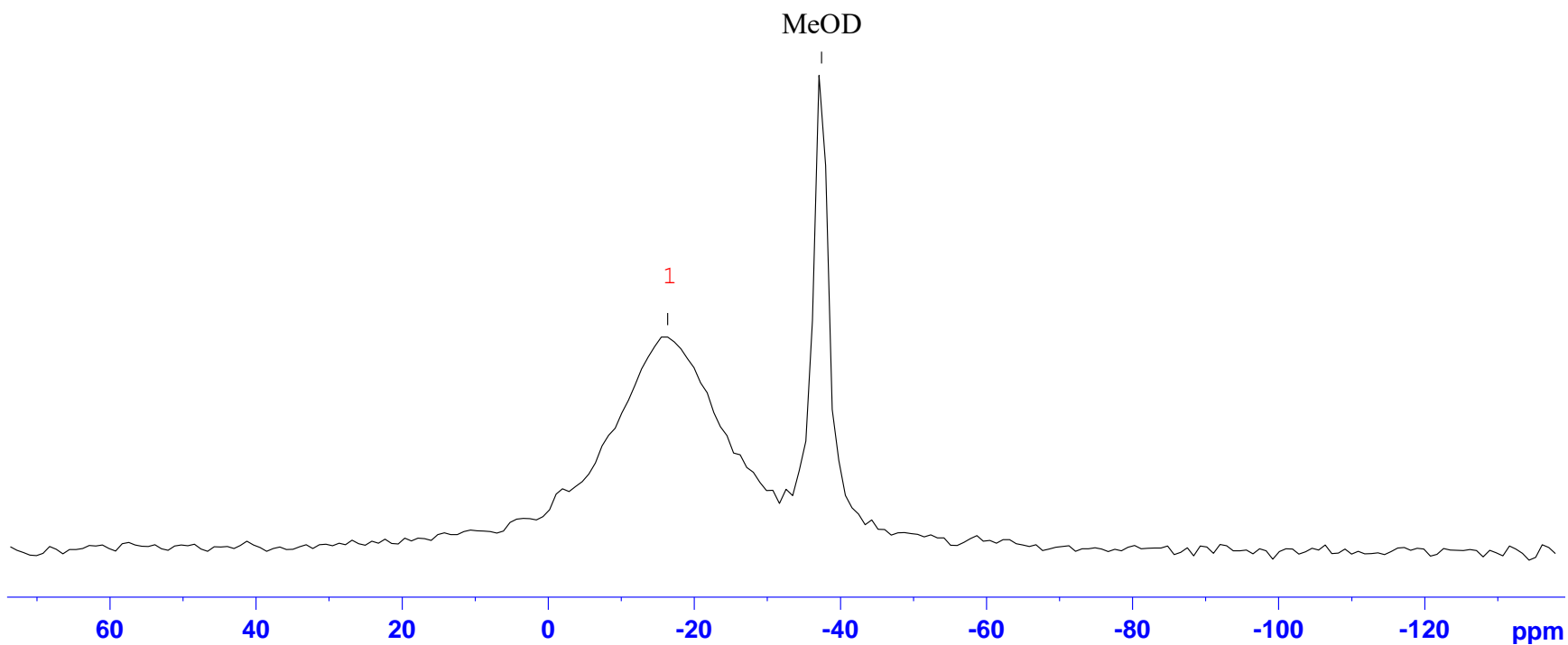
Figure A-11. ^{17}O NMR of 1, 2-O-Isopropylidene-α-D-[6-^{17}O] glucofuranose in Methonal-d$_4$ at 11.7 T.
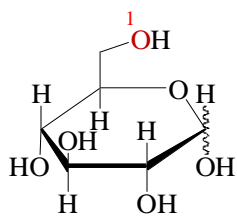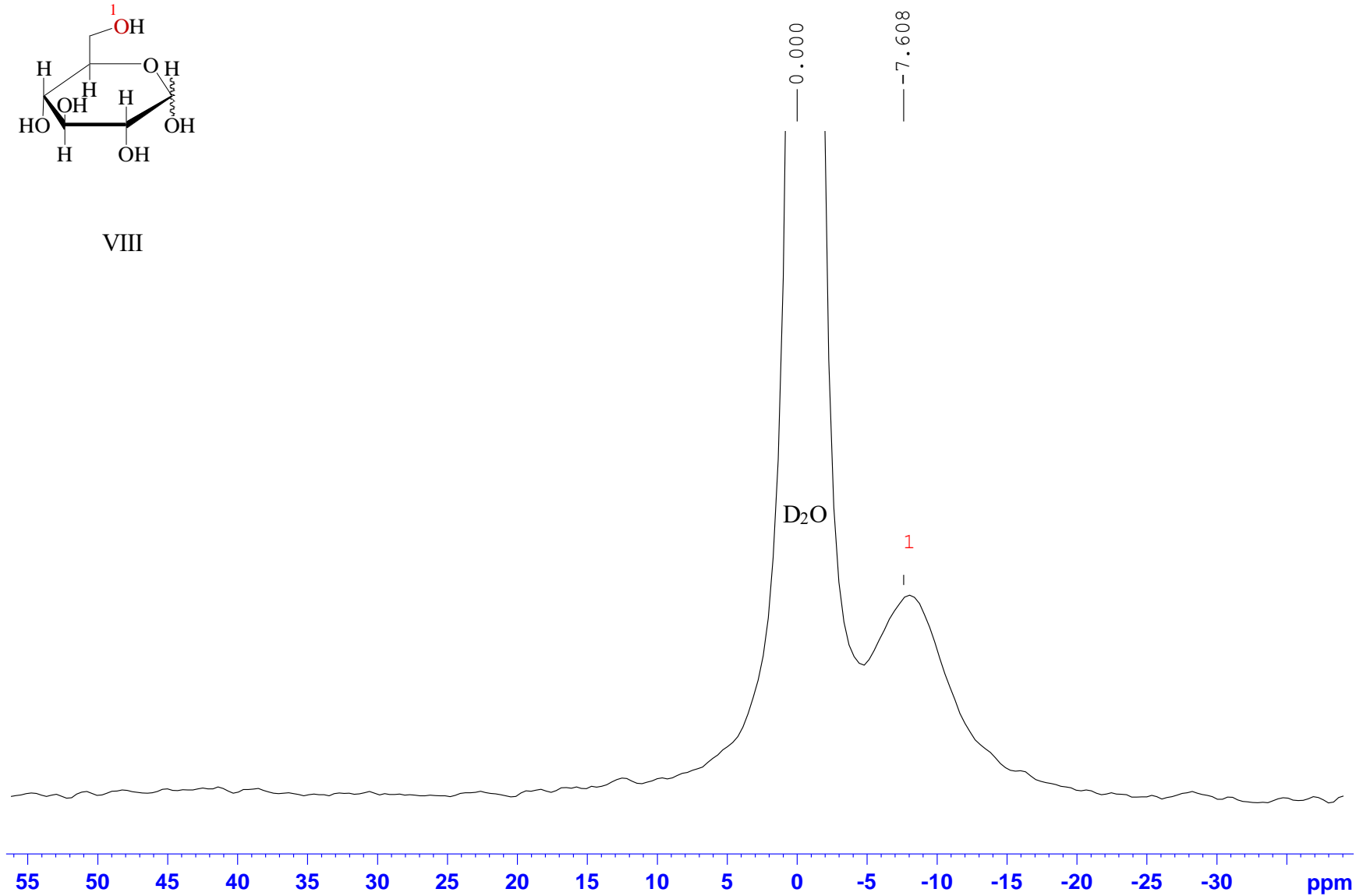
Figure A-12. ^{17}O NMR of D-[6-^{17}O]-glucose in D_2O at 11.7 T, 355 K.

A-12